Published June 13, 2011

ectopic expression of ROP18_F but not KD-ROP18_F led to HA-ATF6β degradation. KD-ROP18_F coprecipitated with ATF6β, as previously observed in the presence of MG132 (Figs. 3 F and 4 C). These results establish a connection between the kinase activity of ROP18 and ATF6β degradation. To examine which portion of the N terminus of ROP18 interacts with ATF6β, vectors expressing the KD versions Δ27- or Δ240-ROP18_F were introduced into 293T cells together with ATF6β. HA-ATF6β coprecipitated with Δ27-KD-ROP18_F but not with Δ240-KD-ROP18_F (Fig. 4 C). To refine the analysis, Δ27ΔN2-ROP18_F was cotransfected and shown to fail to coprecipitate with ATF6β (Fig. 4 D), indicating that the N-terminal 147–164 portion of ROP18 determines the binding to ATF6β. To challenge the possibility that ATF6β is a substrate for ROP18, we performed an in vitro kinase assay using recombinant glutathione *S*-transferase (GST)–tagged ATF6β as a substrate. Immunoprecipitates from 293T cells expressing Flag-tagged ROP18WT, ROP18KD, or ROP16WT were incubated with GST-ATF6β in the presence of radiolabeled ATP. Phosphorylation of GST-tagged ATF6β was detectable in the presence of ROP18WT but not with ROP18KD or ROP16WT (Fig. 4 E). To determine which amino acids on ATF6β are phosphorylated by ROP18, we relied on anti–phospho-Thr (anti-pThr), anti–pSer, and anti–pTyr. GST-tagged ATF6β was detected only in the presence of ROP18WT with anti-pThr, whereas anti–pSer and anti-pTyr gave no signal (Fig. 4 F and not depicted). In contrast, anti-pTyr detected autophosphorylation of ROP16WT (Fig. 4 F), correlating with the Tyr kinase activity of ROP16 (Yamamoto et al., 2009; Ong et al., 2010). Collectively, these results show that ROP18 phosphorylates at least one Thr residue on ATF6β, which leads to its degradation.

The C-terminal portion of ATF6β associates with ROP18

To characterize the region on ATF6β implicated in binding to ROP18, deletion mutants of ATF6β lacking both the transmembrane and the C-terminal portion (ΔCΔTM) or the C terminus alone (ΔC) were generated (Fig. 5 A). Activation of the UPRE-containing reporter by ΔCΔTM-ATF6β was unaffected by the presence of ROP18_F, even at high doses (Fig. 5 B). Moreover, KD-ROP18_F coprecipitated with the HA-tagged full-length ATF6β but not with the ΔC form (Fig. 5 C), suggesting that the C-terminal portion of ATF6β is implicated in the association with ROP18. Intriguingly, the family members of ATF6 proteins are anchored in the membrane of the ER with their C-terminal region predicted to localize in the lumen (Stirling and O'Hare, 2006). If this topology holds true for ATF6β, it would imply that ROP18 needs to gain access to ATF6β in the host ER. To examine whether ROP18 localizes to the ER, YFP-tagged ATF6β and T2A_CFP-tagged KD-ROP18 were bicistronically cloned and coexpressed with an ER-localized RFP in 293T cells (Fig. S5, A and B). Live microscopy revealed colocalization of ER-localized RFP and CFP-ROP18, suggesting that ROP18 is in close proximity with ER-resident proteins. The host ER has recently been reported to fuse with the PV membrane (PVM; Sinai et al., 1997; Goldszmid et al., 2009), and thus it is plausible that ER-localized ATF6β in the vicinity of PVMs might be targeted by ROP18. Indeed, when HFFs infected with parasites were analyzed by electron microscopy, PVMs not only associated with, but also appeared to directly fuse with the host ER (Fig. S5 C). These results indicate that the functional ROP18 kinase is necessary to trigger degradation of ATF6β and suggest that ROP18 might colocalize with ATF6β in the host ER or at the PVM.

Defensive function of ATF6β against infection of *rop18-KO* parasites

Given the correlation between the ability of ROP18 to induce ATF6β degradation and manifestation of virulence in type I parasites, we hypothesized that mice infected with *rop18-KO* parasites are resistant, at least in part, because of a protective effect dependent on ATF6β. To test this possibility under physiological conditions, we generated mice lacking the *Atf6β* gene (Fig. S6, A–C). Homozygous mice with the *Atf6β*-deleted allele were born at the expected Mendelian ratio and grew healthy in specific pathogen–free conditions, as previously reported for another line of ATF6β-deficient mice (Yamamoto et al., 2007). In terms of the cellularity of immune cells under unstimulated conditions, ATF6β-deficient mice behaved similarly to WT mice (unpublished data). When

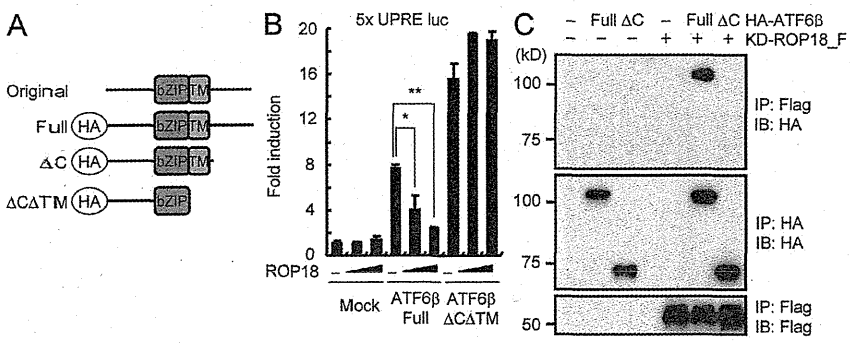

Figure 5. The C-terminal portion of ATF6β interacts with ROP18. (A) HA-tagged ATF6β variants. bZIP, basic Leu zipper; TM, transmembrane. (B) 293T cells were transfected with the ATF6β-dependent luciferase reporter together with the indicated expression vectors. Luciferase activities were expressed as fold increases over the background levels as shown by lysates prepared from mock-transfected cells. Error bars represent means ± the variation range of duplicates. *, $P < 0.03$; **, $P < 0.001$. (C) Lysates of 293T cells transiently cotransfected with 2 μg of the indicated Flag-tagged ROP18 and/or 2 μg of the indicated HA-tagged ATF6β expression vectors were immunoprecipitated with the indicated antibodies and detected by Western blot. IB, immunoblot; IP, immunoprecipitation. (B and C) Data are representative of three (C) or two (B) independent experiments.

Published June 13, 2011

challenged with parasites, ATF6β-deficient mice were more susceptible to *rop18-KO* parasites than WT mice (Fig. 6 A). In sharp contrast, the susceptibility of both genotypes of mice infected with WT parasites was comparable (Fig. S6 D). Moreover, ATF6β-deficient mice similarly succumbed to infection with complemented *rop18-KO* parasite lines (Fig. S6 E). The CTG strain was used as a natural *rop18-KO* parasite and shown to cause a higher mortality rate in ATF6β-deficient mice than in WT mice (Fig. S6 F). To follow more accurately the course of infection, WT and ATF6β-deficient mice were infected with 10^3 luciferase-expressing *rop18-KO* parasites, and the kinetics of infection were monitored by in vivo imaging. Marked increments of *rop18-KO* parasites were observed at days 5, 7, and 8 in ATF6β-deficient mice compared with WT mice (Fig. 6, B and C). To assess whether type I immune responses in ATF6β-deficient mice were affected, the T cell responses were examined at day 6 after infection with *rop18-KO* parasites. The cellularities after the parasite challenges were unchanged in WT and ATF6β-deficient mice (unpublished data). Under these conditions, a significantly reduced IFN-γ response to anti-CD3 was observed in CD8 T cells but not in CD4 T cells (Fig. 6 D). Next, we examined whether the defective IFN-γ production from ATF6β-deficient cells is intrinsic or extrinsic to CD8 T cells. WT DCs were infected with irradiated *rop18-KO* parasites in vitro, and then intraperitoneally injected into WT or ATF6β-deficient mice. 6 d after the injection, splenic CD4 and CD8 T cells were isolated and co-cultured with WT DCs noninfected or infected with *rop18-KO* parasites, and the supernatants were analyzed for IFN-γ production. Comparable IFN-γ production was observed in WT and ATF6β-deficient CD8 T cells, suggesting that the defective IFN-γ production in ATF6β-deficient CD8 T cells may be extrinsic to the T cells (Fig. 6 E). Next, to test whether APCs determine the phenotype, we collected splenic T cells from WT mice infected with *rop18-KO* parasites 6 d after infection and co-cultured with WT or ATF6β-deficient DCs noninfected or infected with *rop18-KO* parasites. We found that CD8 T cells with the infected ATF6β-deficient DCs produced significantly lower amounts of IFN-γ than those with WT DCs (Fig. 6 F). Thus, ATF6β in DCs is responsible for the CD8 T cell–mediated host defense against *rop18-KO* parasites.

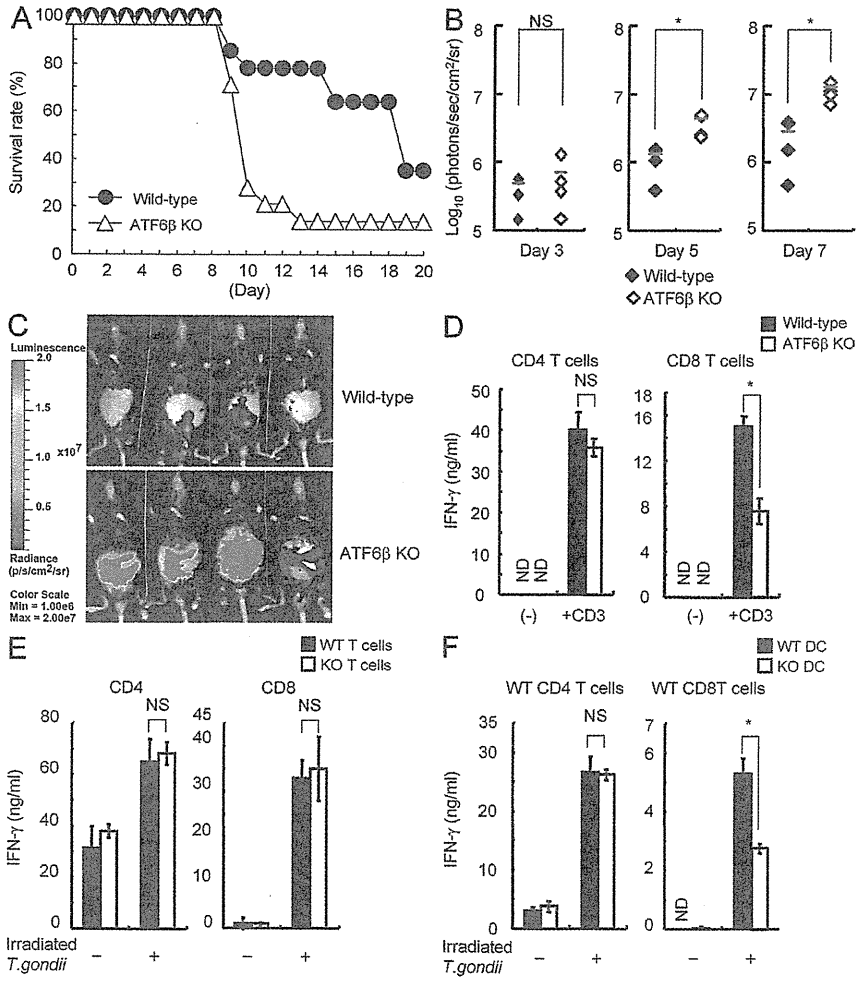

Figure 6. ATF6β functions as a host-defensive protein against *rop18-KO* parasites. (A) WT ($n = 14$) or ATF6β-deficient ($n = 14$) mice were infected with 10^3 *rop18-KO* parasites, and the survival rates were monitored for 20 d. (B) Total photon emission analysis from WT or ATF6β-deficient mice ($n = 4$) infected with 10^3 *rop18-KO* luciferase-expressing parasites at days 3, 5, or 7 after infection. Abdominal photon emission was assessed during a 60-s exposure. The red bars show means of the four samples. *, $P < 0.05$. (C) WT or ATF6β-deficient mice ($n = 4$) were infected with 10^3 *rop18-KO* luciferase-expressing parasites, and the progress of the infection was assessed by bioluminescence imaging at day 8 after infection. Color scales indicate photon emission during a 60-s exposure. (D) CD4 or CD8 T cells from WT or ATF6β-deficient mice ($n = 4$) were cultured in the presence of 5 μg/ml plate-bound anti-CD3 for 24 h. (E) WT DCs infected with irradiated *rop18-KO* parasites were injected into WT or ATF6β-deficient mice. 6 d after DC injection, CD4 or CD8 T cells purified from the spleens were restimulated with DCs uninfected or infected with *rop18-KO* parasites for 48 h. (F) CD4 or CD8 T cells purified from WT mice infected with *rop18-KO* parasites 6 d after infection were restimulated with WT or ATF6β-deficient DCs uninfected or infected with *rop18-KO* parasites for 48 h. (D–F) Concentration of IFN-γ in the culture supernatants was measured by ELISA. Indicated values are means ± SD of triplicates. *, $P < 0.05$. ND, not detected. (A–F) Data are representative of two (B–F) or a cumulative percentage of three (A) independent experiments.

Published June 13, 2011

ATF6β-independent response to the parasite infection

ΔN2-ROP18_F, which are insensitive to the ATF6β-mediated host response, moderately restored in vivo virulence (Fig. 1 G), suggesting that ATF6β-independent host responses may be functional to eliminate the parasites. Because ROP18 is shown to inactivate IRGs by the direct Thr phosphorylation (Fentress et al., 2010; Steinfeldt et al., 2010), we postulated the involvement of IRGs in the moderate host resistance in WT mice infected with *ΔN2-ROP18_F*. To assess whether ΔN2-ROP18 inactivates IRG, macrophages treated with IFN-γ were infected with *ROP18_F*, *ΔN2-ROP18_F*, *KD-ROP18_F*, or *EMPTY* parasites, and the interaction of an IRG Irgb6 with the ROP18 variants was examined by an immunoprecipitation assay (Fig. 7 A). ΔN2-ROP18_F as well as ROP18_F and KD-ROP18_F associated with Irgb6 in inflammatory macrophages. Next, we tested whether ΔN2-ROP18 mediates Thr phosphorylation on Irgb6 by an in vitro kinase assay. Immunoprecipitates of parasites expressing ΔN2-ROP18_F and ROP18_F but not KD-ROP18_F induced Thr phosphorylation of Myc-Irgb6-YFP but not Myc-YFP (Fig. 7 B and not depicted), indicating that activity of the IRG can be blocked by ΔN2-ROP18. Finally, to more carefully dissect contribution of the ATF6β-independent host response, ATF6β-deficient mice were infected with *rop18-KO* parasites complemented with ROP18 variants at a low dose (10^2 tachyzoites), and the parasite loads in the peritoneal cavities and IFN-γ production from splenic T cells were examined. Although the parasite number in mice infected with *Empty vector* was less than those in mice with *ROP18_F* or *ΔN2-ROP18_F* parasites at day 3 after infection, it was almost comparable at day 6. In contrast, the number of parasites in mice infected with *KD-ROP18_F* was consistently lower throughout the course of the experiment (Fig. 7 C). In terms of IFN-γ production, although the CD8 T cell–mediated production was unaltered, the production from CD4 T cells in mice infected with *ROP18_F* or *ΔN2-ROP18_F* was markedly reduced compared with that in mice with *KD-ROP18_F* or *Empty vector* (Fig. 7 D). Thus, these results suggest that the ATF6β-independent response regulates CD4 T cell–mediated IFN-γ production against *rop18-KO* parasites.

DISCUSSION

In this study, we provide the first genetic and biochemical evidence that the host cellular protein, ATF6β, is targeted for degradation by ROP18, a key virulence factor in *T. gondii*. ATF6β is a member of the ATF6-related family of transcription factors that have been shown to operate in the UPR (Yoshida et al., 2001; Yamamoto et al., 2007). Recently, UPR-related molecules such as XBP-1 in *Caenorhabditis elegans* or mammals and a plant ATF6-related molecule were shown to be involved in host

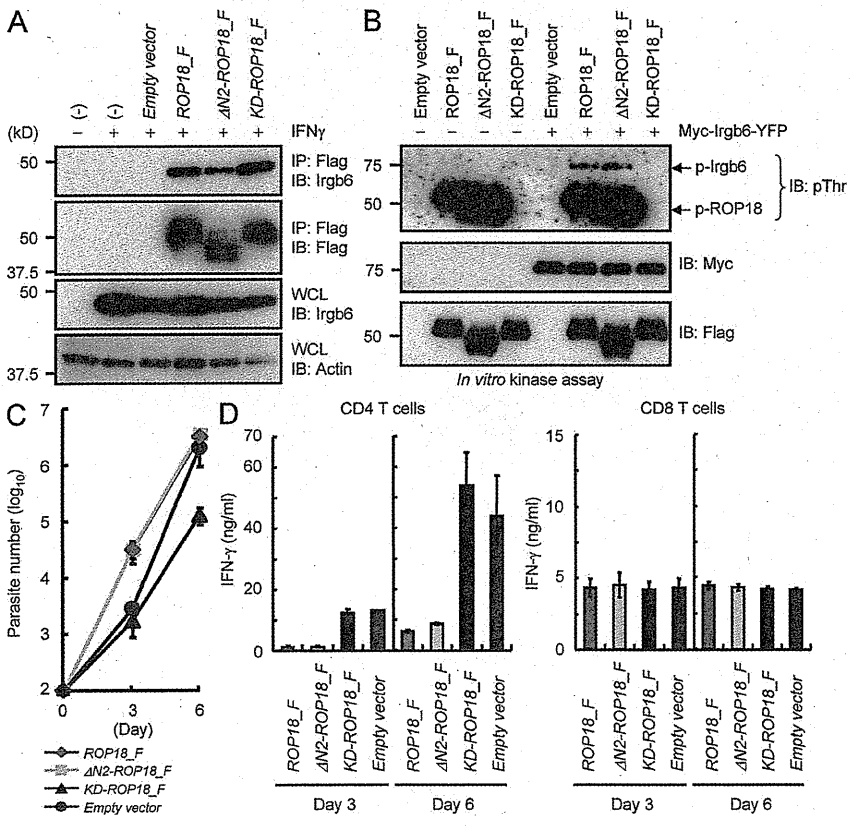

Figure 7. Parasite-induced ATF6β-independent host response. (A) Peritoneal macrophages treated with 30 ng/ml IFN-γ for 24 h were infected with the indicated parasites. Lysates of the infected cells were immunoprecipitated with anti-Flag and detected by Western blot with the indicated antibodies. IB, immunoblot; IP, immunoprecipitation; WCL, whole cell lysate. (B) 293T cells were transiently transfected with empty or Myc-tagged Irgb6-YFP vectors. Cell lysates were immunoprecipitated with anti-Myc and subjected to an in vitro kinase reaction in the presence of anti-Flag immunoprecipitates of the indicated parasites. Proteins were separated on SDS-PAGE, followed by Western blot to analyze Irgb6 phosphorylation or the autophosphorylation of ROP18. For detection of phosphorylated or unphosphorylated Myc-Irgb6-YFP and Flag-tagged proteins by Western blot, anti-pThr, anti-Myc, and anti-Flag were used, respectively. (C and D) ATF6β-deficient mice ($n = 3$) intraperitoneally infected with a dose of the indicated 10^2 parasites. Peritoneal fluids were collected at the indicated days after infection, and the parasite numbers were counted by plaque forming assays (C). CD4 or CD8 T cells from spleens of mice infected with the indicated parasites were cultured in the presence of 5 μg/ml plate-bound anti-CD3 for 24 h. Concentration of IFN-γ in the culture supernatants was measured by ELISA. Indicated values are means ± SD of triplicates. (A–D) Data are representative of two independent experiments.

Published June 13, 2011

defense against pathogens (Tateda et al., 2008; Martinon et al., 2010; Richardson et al., 2010). In this study, we report the protective effect of ATF6β against *rop18-KO* but not WT parasite infection. It remains to be determined whether ATF6β also participates in host defense against other pathogens and whether other ATF6 family members including ATF6α and Creb3 (also known as Luman) are targeted by ROP18 (Liang et al., 2006; Zhang and Kaufman, 2008).

Our data suggest that ATF6β deficiency in DCs rather than in T cells is responsible for the defective production of IFN-γ in CD8 T cells, yet a formal proof would require the conditional ablation of ATF6β in these cell types. Given that ATF6β acts as transcription factor, it will be important to determine which of the ATF6β-regulated genes mediate DC activation leading to CD8 T cell responses.

DCs treated with an inhibitor of the ER-associated degradation (ERAD) system were shown to fail to induce CD8 T cell response by cross-presentation (Goldszmid et al., 2009). The close association and possible fusion of host ER with the PV of *T. gondii* could cause an ER overload leading to ERAD activation (Sinai et al., 1997; Goldszmid et al., 2009). Interestingly, the ATF6 family members regulate the transcription of a subset of ERAD components (Wu et al., 2007), so it is conceivable that type I virulent *T. gondii* strains might target ATF6β in DCs (or other APCs such as macrophages) to down-regulate UPR-meditated host defense (Blanchard and Shastri, 2010). The data presented in this study are consistent with the previous findings that (part of) host ERs fuse with PVs during *T. gondii* infection (Goldszmid et al., 2009; Melo et al., 2010). However, studies showing that some ER-resident proteins colocalized with the PVMs do not constitute direct evidence for the host ER–PV fusion, and thus more in depth analysis is required to support this model.

ATF6β-deficient mice are highly susceptible to *rop18-KO* parasites with high parasite burdens possibly caused by defective IFN-γ responses of CD8 T cells. However, T cells from dying ATF6β-deficient mice (for instance, at days 9–10 after infection), in which the spleen was about to be autodigested and partly adhesive to other organs, secreted extremely high concentrations of IFN-γ even under nonstimulated conditions (unpublished data), which is indicative of an overreacting immune responses just before death. Thus, high susceptibility to the parasites might be primarily attributable to the excessive parasite proliferation and terminally dysregulated immune pathology.

Previous studies reported that ROP18-overexpressing parasites exhibited accelerated growth (Taylor et al., 2006; El Hajj et al., 2007). In contrast, the *rop18-KO* parasites showed normal intracellular growth in this study. It is plausible that overexpression of ROP18 impacts proliferation by acting on additional host cell substrates that are not essential to promote normal growth of *rop18-KO* parasites.

Expression of ΔN2-ROP18_F, which lacks the ATF6β-binding region, moderately restores the virulence of *rop18-KO* parasites. Because this ROP18 mutant does not associate with ATF6β, ATF6β-mediated host defense might be functional in *ΔN2-ROP18_F* parasite infection. Nevertheless, *ΔN2-ROP18_F* parasites are not avirulent, indicating the existence of an additional ROP18-mediated but ATF6β-independent virulence mechanism. ΔN2-ROP18_F lacks 17 aa in the N terminus of ROP18, which corresponds to helix 2 of the ROP5 N-terminal extension that is essential for its localization to the PV (Reese and Boothroyd, 2009). Similarly, ROP18 is injected into the host cytosol during invasion and is ultimately found at the PV (Boothroyd and Dubremetz, 2008). The *ΔN2-ROP18_F* strain might incapacitate ATF6β-independent innate immune responses, including IRG-mediated resistance which is operative soon after the parasite invasion (Hunn et al., 2008; Zhao et al., 2009; Khaminets et al., 2010). Indeed, ROP18 has recently been shown to target the member of IRGs, Irgb6 (Fentress et al., 2010; Steinfeldt et al., 2010). In this study, we characterized ATF6β-independent immune responses in ATF6β-deficient mice infected with *ΔN2-ROP18_F*, which inactivated Irgb6. Compared with infection of *EMPTY* or *KD-ROP18_F*, *ΔN2-ROP18_F* infection resulted in much reduced CD4 T cell–mediated IFN-γ production, suggesting that IRGs may be involved in activation of the ATF6β-independent CD4 T cell response. However, this assumption is contradictory to previous findings that the Stat1–IRG axis is not required for the development of Th1 immunity (Taylor et al., 2000; Collazo et al., 2001; Lieberman et al., 2004). This may be caused by strain-dependent differential host innate immune responses (Robben et al., 2004). Previous studies used type II parasites, whereas this study used type I parasites. IRG-deficient mice with high numbers of type II parasites are shown to culminate in higher concentrations of IL-12 in vitro and in vivo than that in WT mice, possibly leading to the development of apparently normal Th1 immunity that can compensate for the defect in the potential IRG-mediated CD4 T cell phenotype (Taylor et al., 2000; Collazo et al., 2001). Alternatively, the other ATF6β/IRG-independent ROP18-mediated effector mechanisms may suppress the CD4 T cell response. It is of interest in the future to revisit the potential involvement of IRGs in the development of CD4 T cell response using relatively immune-silent but IRGs-sensitive type I *rop18-KO* or type III parasites.

Despite the CD4 T cell–mediated IFN-γ production and the successful suppression of *rop18-KO* parasite (*Empty vector*) increment at the early stage after infection, ATF6β-deficient mice allowed the parasites to proliferate at the late stage and eventually succumbed. The CD8 T cell–mediated response is defective in ATF6β-deficient mice. Moreover, mice deficient in CD8 but not CD4 T cell functions are highly susceptible to acute toxoplasmosis (Casciotti et al., 2002; Combe et al., 2005; Lu et al., 2009). Therefore, even though the ATF6β-independent mechanism activates the CD4 T cell–mediated immunity that contributes to host resistance at early stages, it might be ultimately incompetent to counteract the acute parasite infection under condition of the defective CD8 T cell responses. In contrast, considering that the *rop18-KO* parasites (*Empty vector*) are not as virulent as the *ΔN2-ROP18_F* in WT mice, the ATF6β-independent CD4 T cell response

Published June 13, 2011

may considerably enhance host resistance under the normal CD8 T cell conditions. Previous studies established that interference with the innate function of Irgb6 is an important mechanism of ROP18-mediated virulence especially at an early stage after infection (Fentress et al., 2010; Steinfeldt et al., 2010). Furthermore, our study reveals that ROP18 also targets ATF6β-dependent CD8 T cell–mediated acquired immune responses that act at a later stage after infection. Thus, ROP18 may continue to disarm host immunity during the acute pathogenesis by targeting different host factors at each stage.

In conclusion, this study identifies ATF6β as a novel and unexpected substrate for ROP18. This finding nicely complements the recently published study to establish that the kinase activity of ROP18 is essential for the mortality phenotype and may be required for the suppression of both the ATF6β-dependent and -independent host defense mechanisms (Taylor et al., 2006). Interestingly, KD-ROP18_F expression in *rop18-KO* parasites appeared to reduce virulence. Because ROP18 belongs to the ROP2 subfamily consisting of >30 members including 17 active kinases (Peixoto et al., 2010), it is possible that expression of KD-ROP18 might have a dominant-negative effect, suppressing the action of other family members implicated in virulence. Whether other ROP2 subfamily members are important for the type I parasite–mediated virulence in concert with ROP18 should be examined in the future. Intriguingly, type II parasites are shown to be avirulent in spite of normal expression levels of ROP18. Given that ROP16 does not act positively in the virulence (Saeij et al., 2006), type II parasites might be defective in other ROP2 subfamily members.

In summary, ATF6β has been associated in this study for the first time with a resistance mechanism against an intracellular pathogen. ROP18, an effector molecule that constitutes the major virulence factor *T. gondii* type I strain, controls ATF6β degradation. In the future, the in vitro assay system based on the UPR-containing reporter may facilitate the development of a new pharmaceutical drug targeting ROP18 that can block acute toxoplasmosis.

MATERIALS AND METHODS

Cells, mice, and parasites. BALB/c and outbred CD1 ICR mice (6–8 wk old) were obtained from SLC. All animal experiments were conducted with the approval of the Animal Research Committee of the Graduate School of Medicine at Osaka University. RHΔhxgprt and its derivatives of *T. gondii* were maintained in Vero or HFFs by biweekly passage in RPMI (Nacalai Tesque) supplemented with 2% heat-inactivated FCS (JRH Biosciences), 100 U/ml penicillin, and 0.1 mg/ml streptomycin (Invitrogen). The CTG strain was provided by D. Sibley (Washington University School of Medicine, St. Louis, MO) and maintained in Vero cells in the RPMI media.

Reagents. Antibodies against *T. gondii* major surface antigen 1 (SAG1), anti-TGTP (Irgb6), anti-Myc, and HA probe were obtained from Santa Cruz Biotechnology, Inc. Anti-pTyr and anti-pThr were obtained from Cell Signaling Technology. Anti-Flag and anti-pSer were obtained from Sigma-Aldrich. Anti-ROP1 was provided by J.F. Dubremetz (Université de Montpellier 2, Montpellier, France). For indirect immunofluorescence, anti-HA rat antibody was obtained from Roche. MG132 was obtained from EMD.

Generation of RHΔhxgprt *T. gondii*–expressing OVA and a fusion protein of RFP and luciferase. To express luciferase, RFP, and OVA, we constructed a plasmid harboring p30-OVA and luciferase-RFP fusion proteins (pOVRFPluc). The luciferase and RFP fragments were obtained by PCR using primers OVA_F and OVA_R, with plasmid pGL3 as the template or primers RFP_F and RFP_R using pDsRed-express (Takara Bio Inc.) as the template, respectively. The information for all primers used in this study is listed in Table S1. The EcoRI–XhoI fragment of luciferase and the XhoI–PacI fragment of RFP were cloned into the EcoRI–PacI-digested sag1-ROP16HA-3UTR plasmids (Yamamoto et al., 2009). The NotI fragment of sag1-Luciferase/RFP-3UTR was cloned into the site of p30-OVA plasmids (a gift from D.S. Roos, University of Pennsylvania, Philadelphia, PA), leading to the generation of the OVRFPluc plasmid. 100 μg of the OVRFPluc plasmids was transfected with RHΔhxgprt parasites, and the stable transformants were selected in RPMI media containing 20 μM chloramphenicol (Nacalai Tesque), as p30-OVA plasmids contained a cassette for the chloramphenicol resistance gene (Pepper et al., 2004). RFP-positive parasites were selected by fluorescent microscopy and tested for in vitro and in vivo luciferase activity. Three clones were isolated, and we observed comparable in vitro growth and in vivo virulence to each other and the parental line. Whether the parasite line, which was used for generation of *rop18-KO* parasites, expresses OVA has not been tested in this study.

Generation of ROP18-deficient type I *T. gondii*. Genomic DNA containing the *ROP18* gene was isolated by PCR using primers R18KOLA_F and R18KOLA_R to generate a 5.0-kb-long fragment. Primers R18KOSA_F and R18KOSA_R generated a 1.0-kb fragment. The gene encoding *T. gondii ROP18* consists of a single exon. The targeting vector (pKO-ROP18) was constructed by replacing the entire coding sequence of *ROP18* with the *HXGPRT* gene expression cassette (p2855). Outside the targeting vector, a YFP expression vector was ligated using a NotI site for the negative selection of random integration. 100 μg of the targeting vector linearized by ScaI was transfected into tachyzoites of the normal RHΔhxgprt parental strain or OVRFPluc RHΔhxgprt parasites as previously described (Yamamoto et al., 2009). After 25 μg/ml mycophenolic acid (MPA; Sigma-Aldrich) and 25 μg/ml xanthine (Wako Chemicals USA) selection for 14 d, MPA/xanthine-resistant colonies were sorted using a FACSAria (BD) to isolate YFP-negative parasites. The MPA/xanthine-resistant and YFP-negative parasites were subjected to limiting dilution to isolate the clones. A total of 142 clones were selected and screened by PCR for detecting homologous recombinants using primers DHFRrc01 (from the DHFR promoter of the *HXGPRT* expression vector) and R18ex01 (genomic sequence outside the short fragment of the *ROP18* locus), to detect homologous recombinants. This resulted in the isolation of four clones using normal RHΔhxgprt parasites and two homologous recombinants using OVRFPluc RHΔhxgprt parasites. Subsequently, genomic DNA of WT and ROP18-deficient parasites was extracted and subjected to Southern blot analysis using a DNA probe, which was generated by PCR using primers SB_F and SB_R. Additionally, to confirm the disruption of the gene encoding ROP18, we analyzed total RNA from WT and *rop18-KO* parasites by Northern blot using a DNA probe, which was generated by PCR using primers NB_F and NB_R.

Mammalian expression plasmids. The C-terminal Flag-tagged fragments of ROP18 lacking the N-terminal signal peptide were amplified using primers R18frg2common_F and R18frg2common_R. The series of ROP18 variants were amplified using primers R18D27frg1_F for Δ27, R18D240frg1_F for Δ240, primers for Δ27ΔN2 described in Table S1, and the common primer using genomic DNA from the RH strain and were ligated into the BamHI and NotI sites of a pcDNA vector. The kinase-inactive ROP18 mutant containing point mutations was generated using the primers D394A_F and D394A_R, and expression plasmids were generated using a site-directed mutagenesis kit (Agilent Technologies). The sequences of all constructs were confirmed with a genetic analyzer (ABI PRISM;Applied Biosystems). Human ATF6β cDNA was amplified using primers ATF6β_full_R for Full, ATF6β_DC_R for ΔC, ATF6β_DCDTM_R for ΔCΔTM, and the common primer

Published June 13, 2011

ATF6β_common_F using human BM cDNA as the template and then ligated into the EcoRI and NotI sites of a pcDNA vector for the N-terminal HA-tagged proteins (Invitrogen). Murine Irgb6 cDNA was amplified using primers Irgb6_F and Irgb6_R using IFN-γ–treated mouse macrophage cDNA as the template and then ligated into the EcoRI and XhoI sites of a pcDNA vector for the N-terminal HA-tagged and C-terminal YFP-tagged proteins. To express HA-hATF6β and CFP bicistronically using a self-cleavage T2A peptide (Holst et al., 2006), an expression vector for HA-hATF6β_T2ACFP was generated by ligation with a pcDNA vector for the N-terminal HA and EcoRI–XhoI fragment of hATF6β, which was generated by PCR using primers ATF6β_common_F and ATF6β_full_XhoI_R. T2ACFP was generated by PCR using primers T2ACFP_R and T2ACFP_F using a CFP vector as the template. The expression vector for HA_hATF6β_YFP-T2ACFP_KDROP18_Flag was constructed by cloning the EcoRI–XhoI fragment of hATF6β. The SalI–SacI fragment of YFP was amplified using primers YFP_F and YFP_R, using a YFP vector as the template. The SacI–BamHI fragment of T2ACFP and the BamHI–NotI fragment of KD-ROP18-Flag were inserted into the EcoRI–NotI site of the pcDNA vector for the N-terminal HA tag. By placing the T2A peptide between HA-hATF6β (or HA-hATF6β-YFP) and CFP (or CFP-KD-ROP18-Flag), we obtained independent and reliable expression of both proteins. The ER-localizing RFP vector pDsRed2-ER was purchased from Takara Bio Inc.

Generation of transgenic parasites. To complement the *rop18-KO* parasites, we generated an N-terminal signal peptide–containing ROP18, capable of being processed in the parasite, by PCR using the primer ParasiteR18frg1_F for ROP18-Flag (ROP18_F) or KD-ROP18_F and expressed the ROP18-F proteins driven by the sag1 promoter containing a pyrimethamine resistant gene cassette in the *rop18-KO* strain (Yamamoto et al., 2009). ΔN2-ROP18 lacking residues 147–164 of the N-terminal portion was generated by ligation of two fragments: one from the EcoRI–NotI fragment of ROP18_F and the other generated using primers ParasiteR18frg1F, DN2(ΔHX2)_F, and DN2(ΔHX2)_R. We generated this vector by digesting the pyrimethamine resistance cassette of the p2854 plasmid with NotI and XhoI and ligated this into a Klenow-treated pBluescript sag1-ROP18_F vector. A series of ROP18_F vectors or the empty p2854 vector for the generation of the *Empty vector* strain were transfected into tachyzoites of the *rop18-KO* parasites. We selected for parasites stably expressing the complemented ROP18_F constructs using 3 μM pyrimethamine (Sigma-Aldrich) selection and subjected these to limiting dilution as described previously (Yamamoto et al., 2009).

Generation of ATF6β-deficient mice. The *Atf6β* gene was isolated from genomic DNA extracted from embryonic stem cells (V6.5) by PCR using LA Taq (Takara Bio Inc.). The targeting vector (pKOATF6β) was constructed by replacing a 3.0-kb fragment encoding the exons of ATF6β with a neomycin-resistance gene cassette (*neo*) and a herpes simplex virus thymidine kinase gene driven by the PGK promoter, for negative selection. Genomic DNA containing the murine *Atf6β* gene was isolated by PCR amplification using primers ATF6βKO_LA_F and ATF6βKO_LA_R to generate a 5.0-kb fragment or primers ATF6βKO_SA_F and ATF6βKO_SA_R to generate a shorter 1.0-kb fragment. After the targeting vector was transfected into embryonic stem cells, colonies resistant to both G418 and ganciclovir were selected and screened by PCR and Southern blotting. Homologous recombinants were microinjected into C57BL/6 female mice, and heterozygous F1 progenies were intercrossed to obtain ATF6β-deficient mice. ATF6β-deficient mice and their WT littermates from these intercrosses were used for experiments.

Yeast two-hybrid analysis. Yeast two-hybrid screening was performed as described with the Matchmaker two-hybrid system (Takara Bio Inc.). For construction of the bait plasmid, the cDNA fragment coding the N-terminal portion (aa 35–235) of ROP18 was amplified using primers ROP18Y2H_F and ROP18Y2H_R and cloned in frame into the GAL4 DNA-binding domain of pGBKT7. Yeast strain AH109 was transformed with the bait plasmid plus the human BM Mate & Plate cDNA library (Takara Bio Inc.). After the screening of 10^7 clones, we finally obtained 10 positive clones and recovered the pGAD library from individual clones and expanded in *Escherichia coli*. The inserted cDNA was sequenced and characterized with the BLAST program, resulting in the identification of ATF6β (nine clones) and HLA-DPA1 (one clone). Because the number of positive clones of ATF6β was much greater than that of HLA-DPA1 and because HLA-DPA1 was difficult to be linked to the mouse homologue correctly compared with ATF6β, we selected ATF6β in the following study.

Luciferase reporter assay. The 5× UPRE luciferase reporter was generated by the synthesis of a 312-bp fragment containing five tandem ATF6 binding sites (Invitrogen), with the MluI–SalI fragment inserted into the MluI–XhoI site of the pGL3 luciferase reporter as described previously (Wu et al., 2007; Yamamoto et al., 2007). The reporter plasmids were transiently cotransfected into 293T cells with the control *Renilla* luciferase expression vectors using Lipofectamine 2000 reagent (Invitrogen). Luciferase activities of total cell lysates were measured using the Dual-Luciferase Reporter Assay System (Promega) as described previously (Yamamoto et al., 2006).

Statistical analysis. The unpaired Student's *t* test was used to determine statistical significance among experimental data.

Measurement of IFN-γ by ELISA. CD4 and CD8 T cells were obtained by positive selection using anti-CD4 (L3T4) and anti-CD8a (Ly-2) magnetic beads (Miltenyi Biotech) from splenocytes of mice at day 6 after infection with parasites and cultured for 24 h in 96-well plates (10^5 cells per well) precoated with 5 μg/ml anti-CD3 or preincubated with 10^5 BM-derived DCs (BMDCs) pulsed with heat-killed *T. gondii* antigens, which were prepared by incubation of 10^7 parasites at 56°C for 1 h. For the generation of BMDCs, BM cells were isolated from femurs and cultured with RPMI 1640 supplemented with 10% fetal bovine serum and 10 ng/ml GM-CSF (PeproTech) with medium replaced every 2 d. Concentration of IFN-γ in the culture supernatant was measured by ELISA according to the manufacturer's instructions (R&D Systems), as described previously (Yamamoto et al., 2003).

Western blot analysis and immunoprecipitation. The 293T cells and parasites were lysed in a lysis buffer (1% Nonidet P-40, 150 mM NaCl, and 20 mM Tris-HCl, pH 7.5) containing a protease inhibitor cocktail (Roche). The cell lysates were separated by SDS-PAGE and transferred to polyvinylidene fluoride membranes. For immunoprecipitation, cell lysates were precleared with protein G–Sepharose (GE Healthcare) for 2 h and then incubated with protein G–Sepharose containing 1.0 μg of the indicated antibodies for 12 h with rotation at 4°C. The immunoprecipitants were washed four times with lysis buffer and eluted by boiling with Laemmli sample buffer. The eluates were separated by SDS-PAGE, transferred to polyvinylidene fluoride membranes, and subjected to Western blot analysis as described previously (Yamamoto et al., 2004).

Flow cytometric analysis. 2×10^6 splenocytes were stained with PE-conjugated anti-B220, -CD8, or -CD11c, FITC-conjugated anti-CD3ε or -CD4, and APC-conjugated anti-Gr1. Stained cells were analyzed on a FACSCantoII (BD) and using FlowJo Software (Tree Star).

Microscopic analysis. The 293T cells were transfected with 2 μg of expression vectors for HA_ATF6β_YFP-T2ACFP–tagged KDROP18_Flag or ER-DsRed. At 24 h after transfection, cells were analyzed using a fluorescence microscope (IX71; Olympus).

Immunofluorescence analysis. HFF cells infected with parasites were fixed for 8 min in PBS containing 4% paraformaldehyde (PFA)/0.05% glutaraldehyde. Cells were permeabilized with PBS containing 0.2% Triton X-100 (PBS/TX) and then blocked with 2% BSA in PBS/TX. Subsequently, cells were incubated with anti-Rop1 rabbit antibody (1:200) and anti-Flag mouse

Published June 13, 2011

antibody (1:6,000; Sigma-Aldrich) for 1 h at room temperature, followed by incubation with Alexa Fluor 488–conjugated goat anti–rabbit IgG antibody (Invitrogen) and Alexa Fluor 594–conjugated goat anti–mouse IgG antibody (Invitrogen) for 45 min at room temperature in the dark. Finally, the immunostained cells were mounted with Fluoromount-G (SouthernBiotech) on glass slides and analyzed using a fluorescence microscope (Axioskop 2; Carl Zeiss) equipped with a color charge-coupled device camera (Axiocam HR; Carl Zeiss).

Plaque assay. The WT and *rop18-KO* parasites were used to infect monolayers of HFFs seeded in 24-well plates. After incubation for 8–9 d at 37°C, cells were fixed with 4% PFA and 0.05% glutaraldehyde in PBS, followed by staining with Giemsa for 10 min.

Assessment of intracellular growth. Host cells seeded on 24-well immunofluorescence assay plates were inoculated with freshly released WT or *rop18-KO* parasites. At 24 h after infection, parasites were fixed with 4% PFA. Immunofluorescence assays were performed using α-TgGAP45 antibody, and parasites were counted on at least 100 vacuoles for each strain.

Electron microscopy analysis. Monolayers of HFFs were infected with *rop18-KO* parasites. Samples were collected at 4 h after infection and processed for electron microscopy using routine techniques. In brief, parasite pellets were fixed in 2.5% glutaraldehyde in 0.1 M phosphate buffer, post-fixed in osmium tetroxide, dehydrated in ethanol, and treated with propylene oxide before embedding in Spurr's epoxy resin. Thin sections were stained with uranyl acetate and lead citrate before examination with an electron microscope (1200EX; JEOL).

In vivo imaging analysis. Mice were intraperitoneally infected with 10^3 freshly egressed tachyzoites resuspended in 100 µl PBS, with assessment of bioluminescence performed on the indicated days after infection. For the detection of bioluminescence emission, mice were intraperitoneally injected with 3 mg D-luciferin in 200 µl PBS (Promega), maintained for 5 min to allow for adequate dissemination of luciferin, and subsequently anaesthetized with isoflurane (Dainippon Sumitomo Pharma). At 10 min after injection of D-luciferin, photonic emissions were detected using an in vivo imaging system (IVIS 100; Xenogen) and Living image software (Xenogen).

Recombinant ATF6β purification. GST-tagged ATF6β cDNA was subcloned into pFAST-Bac (Invitrogen) for expression in Sf9 insect cells. Proteins were purified in accordance with the manufacturer's instruction as described previously (Yamamoto et al., 2006).

In vitro kinase assay. 5×10^6 293T cells (6-cm dish) were transiently transfected with a total of 4 µg of either empty vector or the indicated plasmids (4 µg of Flag-tagged ROP18WT, ROP18KD, or ROP16WT), using Lipofectamine 2000 as specified by the manufacturer. Cells were harvested 24 h after transfection, lysed, and then immunoprecipitated with protein G–Sepharose together with 1.0 µg anti-Flag M2 mAb (Sigma-Aldrich) for 12 h by rotation. The beads were washed four times with lysis buffer and another three times with kinase assay buffer (30 mM MOPS, pH 7.5, 50 mM NaCl, 10% glycerol, 10 mM $MgCl_2$, and 10 mM $MnCl_2$). The immunoprecipitates were incubated with 1 µg GST-ATF6β and 10 mCi γ-[^{32}P]ATP (GE Healthcare) or 5 µM cold ATP (Wako Chemicals USA) to phosphorylate GST-ATF6β, ROP18WT, ROP18KD, or ROP16WT at 30°C for 30 min. In the experiments for Fig. 7 B, immunoprecipitates of the parasites complemented with the ROP18 variants, which were prepared by immunoprecipitation of the parasite lysates by anti-Flag, were incubated with anti-myc immunoprecipitates of 293T cells transfected with control- or Myc-tagged Irgb6-YFP fusion vectors in the presence with 5 µM cold ATP in the kinase reaction buffer at 30°C for 30 min with gentle agitation. Kinase reactions were stopped by the addition of Laemmli sample buffer and were separated on a 5–20% polyacrylamide gradient gel. For radioactive samples, gel was detained, dried, and exposed to x-ray film. For cold samples, gel was detained and subjected to Western blot to detect unphosphorylated or phospho-GST–tagged ATF6β and Flag-tagged ROP18WT, ROP18KD, or ROP16WT by anti-GST, anti-pThr, anti-pSer, anti-pTyr, and anti-Flag, respectively.

Immunological experiments. To assess the phenotype in T cells (Fig. 6 E), DCs were generated from BMs of two WT mice cultured in GM-CSF. 2×10^7 DCs were collected at day 6 after cultivation and infected with irradiated *rop18-KO* parasites at multiplicity of infection (MOI) = 1 for 12 h. The cells were collected at 1,100 rpm and extensively washed with PBS three times at 4°C. 1,000,000 DCs were intraperitoneally injected into the littermates of WT or ATF6β-deficient mice ($n = 2$ for each group; $n = 4$ total for two independent experiments). 6 d after injection, CD4 or CD8 T cells were isolated by the positive selection of splenic T cells. The T cells (10^5 cells) were co-cultured with WT DCs (5×10^4 cells), which were freshly isolated from the littermate WT mouse and cultivated for 6 d in the presence of GM-CSF and uninfected or infected with irradiated *rop18-KO* parasites for 12 h at MOI = 1 for 48 h. The supernatants were collected and tested for ELISA to measure the IFN-γ concentration.

To analyze the phenotype of DCs for the ability of IFN-γ production from T cells (Fig. 6 F), CD4 and CD8 T cells were isolated from WT mice infected with 10^3 *rop18-KO* parasites 6 d after the infection. The T cells (10^5 cells) were co-cultured with DCs (5×10^4 cells), which were freshly isolated from the littermate WT or ATF6β-deficient mice ($n = 2$ for each group; $n = 4$ total for two independent experiments), and cultivated for 6 d in the presence of GM-CSF and uninfected or infected with irradiated *rop18-KO* parasites for 12 h at MOI = 1 for 48 h. The supernatants were collected and tested for ELISA to measure the IFN-γ concentration.

Quantification of parasite loads. The parasites in the peritoneal cavities were enumerated as described previously (Robben et al., 2005). In brief, total peritoneal contents were collected by injection of 5 ml of FCS-free RPMI into the peritoneal cavities of infected mice. Aliquots of the recovered fluids were added onto confluent monolayer of mouse embryonic fibroblasts in 96-well culture plates with 10-times serial dilutions from 10^0 to 10^5 and 4 wells of each dilution. 4 d after infection, the numbers of plaques were counted to calculate the total parasite numbers in the original peritoneal cavities.

Online supplemental material. Fig. S1 shows parasitological analysis of *rop18-KO* type I *T. gondii*. Fig. S2 demonstrates complementation of *rop18-KO* parasites by various ROP18 mutants. Fig. S3 exhibits splenic cellularity in mice infected with WT or *rop18-KO* parasites. Fig. S4 shows specific interaction of Nt-ROP18 with ATF6β in yeasts and similar infection levels between WT and *rop18-KO* parasites in 293T cells. Fig. S5 demonstrates ER localization of ROP18 and PVM–ER fusion. Fig. S6 describes the strategy for generation of ATF6β-deficient mice and shows comparable susceptibility in WT or ATF6β-deficient mice infected with WT *T. gondii*. Table S1 provides a list of the primers used in this study. Online supplemental material is available at http://www.jem.org/cgi/content/full/jem.20101660/DC1.

We thank C. Hidaka and M. Yasuda for excellent secretarial assistance, Y. Magota for technical assistance, and members of K. Takeda's laboratory for discussions. We are grateful to W. Daher for technical assistance and stimulating discussions. We also thank Professor D. Sibley for providing the CTG strain.

This work was supported by grants from the Ministry of Education, Culture, Sports, Science and Technology, the Strategic International Cooperative Program (Research Exchange Type), the Japan Science and Technology Agency, the Takeda Science Foundation, the Kanae Foundation for the Promotion of Medical Science, the Cell Science Research Foundation, the Ichiro Kanehara Foundation, the Kato Memorial Bioscience Foundation, and the Uehara Memorial Foundation. C. Mueller is supported by the Japanese-Swiss Science and Technology Program.

The authors have no conflicting financial interests to declare.

Submitted: 11 August 2010
Accepted: 23 May 2011

Published June 13, 2011

REFERENCES

Ajzenberg, D., A.L. Bañuls, C. Su, A. Dumètre, M. Demar, B. Carme, and M.L. Dardé. 2004. Genetic diversity, clonality and sexuality in *Toxoplasma gondii*. *Int. J. Parasitol.* 34:1185–1196. doi:10.1016/j.ijpara.2004.06.007

Blanchard, N., and N. Shastri. 2010. Topological journey of parasite-derived antigens for presentation by MHC class I molecules. *Trends Immunol.* 31:414–421. doi:10.1016/j.it.2010.08.004

Boothroyd, J.C., and J.F. Dubremetz. 2008. Kiss and spit: the dual roles of *Toxoplasma* rhoptries. *Nat. Rev. Microbiol.* 6:79–88. doi:10.1038/nrmicro1800

Boothroyd, J.C., and M.E. Grigg. 2002. Population biology of *Toxoplasma gondii* and its relevance to human infection: do different strains cause different disease? *Curr. Opin. Microbiol.* 5:438–442. doi:10.1016/S1369-5274(02)00349-1

Casciotti, L., K.H. Ely, M.E. Williams, and I.A. Khan. 2002. CD8(+)-T-cell immunity against *Toxoplasma gondii* can be induced but not maintained in mice lacking conventional CD4(+) T cells. *Infect. Immun.* 70:434–443. doi:10.1128/IAI.70.2.434-443.2002

Collazo, C.M., G.S. Yap, G.D. Sempowski, K.C. Lusby, L. Tessarollo, G.F. Woude, A. Sher, and G.A. Taylor. 2001. Inactivation of LRG-47 and IRG-47 reveals a family of interferon γ-inducible genes with essential, pathogen-specific roles in resistance to infection. *J. Exp. Med.* 194:181–188. doi:10.1084/jem.194.2.181

Combe, C.L., T.J. Curiel, M.M. Moretto, and I.A. Khan. 2005. NK cells help to induce CD8(+)-T-cell immunity against *Toxoplasma gondii* in the absence of CD4(+)T cells. *Infect. Immun.* 73:4913–4921. doi:10.1128/IAI.73.8.4913-4921.2005

Dardé, M.L. 2008. *Toxoplasma gondii*, "new" genotypes and virulence. *Parasite.* 15:366–371.

Dubremetz, J.F. 2007. Rhoptries are major players in *Toxoplasma gondii* invasion and host cell interaction. *Cell. Microbiol.* 9:841–848. doi:10.1111/j.1462-5822.2007.00909.x

El Hajj, H., E. Demey, J. Poncet, M. Lebrun, B. Wu, N. Galéotti, M.N. Fourmaux, O. Mercereau-Puijalon, H. Vial, G. Labesse, and J.F. Dubremetz. 2006. The ROP2 family of *Toxoplasma gondii* rhoptry proteins: proteomic and genomic characterization and molecular modeling. *Proteomics.* 6:5773–5784. doi:10.1002/pmic.200600187

El Hajj, H., M. Lebrun, S.T. Arold, H. Vial, G. Labesse, and J.F. Dubremetz. 2007. ROP18 is a rhoptry kinase controlling the intracellular proliferation of *Toxoplasma gondii*. *PLoS Pathog.* 3:e14. doi:10.1371/journal.ppat.0030014

Fentress, S.J., M.S. Behnke, I.R. Dunay, M. Mashayekhi, L.M. Rommereim, B.A. Fox, D.J. Bzik, G.A. Taylor, B.E. Turk, C.F. Lichti, et al. 2010. Phosphorylation of immunity-related GTPases by a *Toxoplasma gondii*-secreted kinase promotes macrophage survival and virulence. *Cell Host Microbe.* 8:484–495. doi:10.1016/j.chom.2010.11.005

Goldszmid, R.S., I. Coppens, A. Lev, P. Caspar, I. Mellman, and A. Sher. 2009. Host ER–parasitophorous vacuole interaction provides a route of entry for antigen cross-presentation in *Toxoplasma gondii*–infected dendritic cells. *J. Exp. Med.* 206:399–410. doi:10.1084/jem.20082108

Holst, J., K.M. Vignali, A.R. Burton, and D.A. Vignali. 2006. Rapid analysis of T-cell selection in vivo using T cell-receptor retrogenic mice. *Nat. Methods.* 3:191–197. doi:10.1038/nmeth858

Howe, D.K., and L.D. Sibley. 1995. *Toxoplasma gondii* comprises three clonal lineages: correlation of parasite genotype with human disease. *J. Infect. Dis.* 172:1561–1566. doi:10.1093/infdis/172.6.1561

Hunn, J.P., S. Koenen-Waisman, N. Papic, N. Schroeder, N. Pawlowski, R. Lange, F. Kaiser, J. Zerrahn, S. Martens, and J.C. Howard. 2008. Regulatory interactions between IRG resistance GTPases in the cellular response to *Toxoplasma gondii*. *EMBO J.* 27:2495–2509. doi:10.1038/emboj.2008.176

Joynson, D.H.M, and T.J. Wreghitt, editors. 2001. Toxoplasmosis: A Comprehensive Clinical Guide. Cambridge University Press, Cambridge. 410 pp.

Khaminets, A., J.P. Hunn, S. Könen-Waisman, Y.O. Zhao, D. Preukschat, J. Coers, J.P. Boyle, Y.C. Ong, J.C. Boothroyd, G. Reichmann, and J.C. Howard. 2010. Coordinated loading of IRG resistance GTPases on to the *Toxoplasma gondii* parasitophorous vacuole. *Cell. Microbiol.* 12:939–961. doi:10.1111/j.1462-5822.2010.01443.x

Liang, G., T.E. Audas, Y. Li, G.P. Cockram, J.D. Dean, A.C. Martyn, K. Kokame, and R. Lu. 2006. Luman/CREB3 induces transcription of the endoplasmic reticulum (ER) stress response protein Herp through an ER stress response element. *Mol. Cell. Biol.* 26:7999–8010. doi:10.1128/MCB.01046-06

Lieberman, L.A., M. Banica, S.L. Reiner, and C.A. Hunter. 2004. STAT1 plays a critical role in the regulation of antimicrobial effector mechanisms, but not in the development of Th1-type responses during toxoplasmosis. *J. Immunol.* 172:457–463.

Lu, F., S. Huang, and L.H. Kasper. 2009. The temperature-sensitive mutants of *Toxoplasma gondii* and ocular toxoplasmosis. *Vaccine.* 27:573–580. doi:10.1016/j.vaccine.2008.10.090

Martinon, F., X. Chen, A.H. Lee, and L.H. Glimcher. 2010. TLR activation of the transcription factor XBP1 regulates innate immune responses in macrophages. *Nat. Immunol.* 11:411–418. doi:10.1038/ni.1857

Melo, M.B., P. Kasperkovitz, A. Cerny, S. Könen-Waisman, E.A. Kurt-Jones, E. Lien, B. Beutler, J.C. Howard, D.T. Golenbock, and R.T. Gazzinelli. 2010. UNC93B1 mediates host resistance to infection with *Toxoplasma gondii*. *PLoS Pathog.* 6:e1001071. doi:10.1371/journal.ppat.1001071

Montoya, J.G., and J.S. Remington. 2008. Management of *Toxoplasma gondii* infection during pregnancy. *Clin. Infect. Dis.* 47:554–566. doi:10.1086/590149

Ogawa, M., M. Yamamoto, and K. Takeda. 2010. Role of *Toxoplasma gondii* rhoptry kinase ROP16 in Stat6 activation. *Med. J. Osaka Univ.* 53:1–4.

Ong, Y.C., M.L. Reese, and J.C. Boothroyd. 2010. *Toxoplasma* rhoptry protein 16 (ROP16) subverts host function by direct tyrosine phosphorylation of STAT6. *J. Biol. Chem.* 285:28731–28740. doi:10.1074/jbc.M110.112359

Peixoto, L., F. Chen, O.S. Harb, P.H. Davis, D.P. Beiting, C.S. Brownback, D. Ouloguem, and D.S. Roos. 2010. Integrative genomic approaches highlight a family of parasite-specific kinases that regulate host responses. *Cell Host Microbe.* 8:208–218. doi:10.1016/j.chom.2010.07.004

Pepper, M., F. Dzierszinski, A. Crawford, C.A. Hunter, and D. Roos. 2004. Development of a system to study CD4+-T-cell responses to transgenic ovalbumin-expressing *Toxoplasma gondii* during toxoplasmosis. *Infect. Immun.* 72:7240–7246. doi:10.1128/IAI.72.12.7240-7246.2004

Reese, M.L., and J.C. Boothroyd. 2009. A helical membrane-binding domain targets the *Toxoplasma* ROP2 family to the parasitophorous vacuole. *Traffic.* 10:1458–1470. doi:10.1111/j.1600-0854.2009.00958.x

Richardson, C.E., T. Kooistra, and D.H. Kim. 2010. An essential role for XBP-1 in host protection against immune activation in *C. elegans*. *Nature.* 463:1092–1095. doi:10.1038/nature08762

Robben, P.M., D.G. Mordue, S.M. Truscott, K. Takeda, S. Akira, and L.D. Sibley. 2004. Production of IL-12 by macrophages infected with *Toxoplasma gondii* depends on the parasite genotype. *J. Immunol.* 172:3686–3694.

Robben, P.M., M. LaRegina, W.A. Kuziel, and L.D. Sibley. 2005. Recruitment of Gr-1$^+$ monocytes is essential for control of acute toxoplasmosis. *J. Exp. Med.* 201:1761–1769. doi:10.1084/jem.20050054

Saeij, J.P., J.P. Boyle, S. Coller, S. Taylor, L.D. Sibley, E.T. Brooke-Powell, J.W. Ajioka, and J.C. Boothroyd. 2006. Polymorphic secreted kinases are key virulence factors in toxoplasmosis. *Science.* 314:1780–1783. doi:10.1126/science.1133690

Saeij, J.P., S. Coller, J.P. Boyle, M.E. Jerome, M.W. White, and J.C. Boothroyd. 2007. *Toxoplasma* co-opts host gene expression by injection of a polymorphic kinase homologue. *Nature.* 445:324–327. doi:10.1038/nature05395

Shirahata, T., T. Yamashita, C. Ohta, H. Goto, and A. Nakane. 1994. CD8+ T lymphocytes are the major cell population involved in the early gamma interferon response and resistance to acute primary *Toxoplasma gondii* infection in mice. *Microbiol. Immunol.* 38:789–796.

Sibley, L.D., and J.C. Boothroyd. 1992. Virulent strains of *Toxoplasma gondii* comprise a single clonal lineage. *Nature.* 359:82–85. doi:10.1038/359082a0

Sibley, L.D., and D.K. Howe. 1996. Genetic basis of pathogenicity in toxoplasmosis. *Curr. Top. Microbiol. Immunol.* 219:3–15.

Sinai, A.P., P. Webster, and K.A. Joiner. 1997. Association of host cell endoplasmic reticulum and mitochondria with the *Toxoplasma gondii*

Published June 13, 2011

parasitophorous vacuole membrane: a high affinity interaction. *J. Cell Sci.* 110:2117–2128.

Steinfeldt, T., S. Könen-Waisman, L. Tong, N. Pawlowski, T. Lamkemeyer, L.D. Sibley, J.P. Hunn, and J.C. Howard. 2010. Phosphorylation of mouse immunity-related GTPase (IRG) resistance proteins is an evasion strategy for virulent *Toxoplasma gondii*. *PLoS Biol.* 8:e1000576. doi:10.1371/journal.pbio.1000576

Stirling, J., and P. O'Hare. 2006. CREB4, a transmembrane bZip transcription factor and potential new substrate for regulation and cleavage by S1P. *Mol. Biol. Cell.* 17:413–426. doi:10.1091/mbc.E05-06-0500

Subauste, C.S., and J.S. Remington. 1991. Role of gamma interferon in *Toxoplasma gondii* infection. *Eur. J. Clin. Microbiol. Infect. Dis.* 10:58–67. doi:10.1007/BF01964408

Tateda, C., R. Ozaki, Y. Onodera, Y. Takahashi, K. Yamaguchi, T. Berberich, N. Koizumi, and T. Kusano. 2008. NtbZIP60, an endoplasmic reticulum-localized transcription factor, plays a role in the defense response against bacterial pathogens in *Nicotiana tabacum*. *J. Plant Res.* 121:603–611. doi:10.1007/s10265-008-0185-5

Taylor, G.A., C.M. Collazo, G.S. Yap, K. Nguyen, T.A. Gregorio, L.S. Taylor, B. Eagleson, L. Secrest, E.A. Southon, S.W. Reid, et al. 2000. Pathogen-specific loss of host resistance in mice lacking the IFN-γ-inducible gene IGTP. *Proc. Natl. Acad. Sci. USA.* 97:751–755. doi:10.1073/pnas.97.2.751

Taylor, S., A. Barragan, C. Su, B. Fux, S.J. Fentress, K. Tang, W.L. Beatty, H.E. Hajj, M. Jerome, M.S. Behnke, et al. 2006. A secreted serine-threonine kinase determines virulence in the eukaryotic pathogen *Toxoplasma gondii*. *Science.* 314:1776–1780. doi:10.1126/science.1133643

Wang, Y., J. Shen, N. Arenzana, W. Tirasophon, R.J. Kaufman, and R. Prywes. 2000. Activation of ATF6 and an ATF6 DNA binding site by the endoplasmic reticulum stress response. *J. Biol. Chem.* 275:27013–27020.

Wu, J., D.T. Rutkowski, M. Dubois, J. Swathirajan, T. Saunders, J. Wang, B. Song, G.D. Yau, and R.J. Kaufman. 2007. ATF6α optimizes long-term endoplasmic reticulum function to protect cells from chronic stress. *Dev. Cell.* 13:351–364. doi:10.1016/j.devcel.2007.07.005

Yamamoto, K., T. Sato, T. Matsui, M. Sato, T. Okada, H. Yoshida, A. Harada, and K. Mori. 2007. Transcriptional induction of mammalian ER quality control proteins is mediated by single or combined action of ATF6α and XBP1. *Dev. Cell.* 13:365–376. doi:10.1016/j.devcel.2007.07.018

Yamamoto, M., S. Sato, H. Hemmi, K. Hoshino, T. Kaisho, H. Sanjo, O. Takeuchi, M. Sugiyama, M. Okabe, K. Takeda, and S. Akira. 2003. Role of adaptor TRIF in the MyD88-independent toll-like receptor signaling pathway. *Science.* 301:640–643. doi:10.1126/science.1087262

Yamamoto, M., S. Yamazaki, S. Uematsu, S. Sato, H. Hemmi, K. Hoshino, T. Kaisho, H. Kuwata, O. Takeuchi, K. Takeshige, et al. 2004. Regulation of Toll/IL-1-receptor-mediated gene expression by the inducible nuclear protein IkappaBzeta. *Nature.* 430:218–222. doi:10.1038/nature02738

Yamamoto, M., T. Okamoto, K. Takeda, S. Sato, H. Sanjo, S. Uematsu, T. Saitoh, N. Yamamoto, H. Sakurai, K.J. Ishii, et al. 2006. Key function for the Ubc13 E2 ubiquitin-conjugating enzyme in immune receptor signaling. *Nat. Immunol.* 7:962–970. doi:10.1038/ni1367

Yamamoto, M., D.M. Standley, S. Takashima, H. Saiga, M. Okuyama, H. Kayama, E. Kubo, H. Ito, M. Takaura, T. Matsuda, et al. 2009. A single polymorphic amino acid on *Toxoplasma gondii* kinase ROP16 determines the direct and strain-specific activation of Stat3. *J. Exp. Med.* 206:2747–2760. doi:10.1084/jem.20091703

Yap, G.S., and A. Sher. 1999. Cell-mediated immunity to *Toxoplasma gondii*: initiation, regulation and effector function. *Immunobiology.* 201:240–247.

Yoshida, H., T. Okada, K. Haze, H. Yanagi, T. Yura, M. Negishi, and K. Mori. 2001. Endoplasmic reticulum stress-induced formation of transcription factor complex ERSF including NF-Y (CBF) and activating transcription factors 6α and 6β that activates the mammalian unfolded protein response. *Mol. Cell. Biol.* 21:1239–1248. doi:10.1128/MCB.21.4.1239-1248.2001

Zhang, K., and R.J. Kaufman. 2008. From endoplasmic-reticulum stress to the inflammatory response. *Nature.* 454:455–462. doi:10.1038/nature07203

Zhao, Y., D.J. Ferguson, D.C. Wilson, J.C. Howard, L.D. Sibley, and G.S. Yap. 2009. Virulent *Toxoplasma gondii* evade immunity-related GTPase-mediated parasite vacuole disruption within primed macrophages. *J. Immunol.* 182:3775–3781. doi:10.4049/jimmunol.0804190

OPEN ACCESS Freely available online

PLoS one

Gibberellin Biosynthetic Inhibitors Make Human Malaria Parasite *Plasmodium falciparum* Cells Swell and Rupture to Death

Tomoko Toyama[1,2*¤], Michiru Tahara[3], Kisaburo Nagamune[3], Kenji Arimitsu[4], Yoshio Hamashima[4], Nirianne M. Q. Palacpac[2], Hiroshi Kawaide[5], Toshihiro Horii[2], Kazuyuki Tanabe[1,2*]

1 Laboratory of Malariology, Research Institute for Microbial Diseases, Osaka University, Yamadaoka, Suita, Osaka, Japan, **2** Department of Molecular Protozoology, Research Institute for Microbial Diseases, Osaka University, Yamadaoka, Suita, Osaka, Japan, **3** Department of Parasitology, National Institute of Infectious Diseases, Toyama, Shinjuku-ku, Tokyo, Japan, **4** Pharmaceutical Manufacturing Chemistry, Division of Medicinal Chemical Sciences, Kyoto Pharmaceutical University, Misasagi-Nakauchicho, Yamashinaku, Kyoto, Japan, **5** Institute of Agriculture, Tokyo University of Agriculture and Technology (TUAT), Saiwaicho, Fuchu, Tokyo, Japan

Abstract

Malaria remains as one of the most devastating infectious disease, and continues to exact an enormous toll in medical cost and days of labor lost especially in the tropics. Effective malaria control and eventual eradication remain a huge challenge, with efficacious antimalarials as important intervention/management tool. Clearly new alternative drugs that are more affordable and with fewer side effects are desirable. After preliminary *in vitro* assays with plant growth regulators and inhibitors, here, we focus on biosynthetic inhibitors of gibberellin, a plant hormone with many important roles in plant growth, and show their inhibitory effect on the growth of both apicomplexa, *Plasmodium falciparum* and *Toxoplasma gondii*. Treatment of *P. falciparum* cultures with the gibberellin biosynthetic inhibitors resulted in marked morphological changes that can be reversed to a certain degree under hyperosmotic environment. These unique observations suggest that changes in the parasite membrane permeability may explain the pleiotropic effects observed within the intracellular parasites.

Citation: Toyama T, Tahara M, Nagamune K, Arimitsu K, Hamashima Y, et al. (2012) Gibberellin Biosynthetic Inhibitors Make Human Malaria Parasite *Plasmodium falciparum* Cells Swell and Rupture to Death. PLoS ONE 7(3): e32246. doi:10.1371/journal.pone.0032246

Editor: Gordon Langsley, Institut national de la santé et de la recherche médicale - Institut Cochin, France

Received August 18, 2011; **Accepted** January 24, 2012; **Published** March 7, 2012

Funding: This work was supported by Ministry of Education, Culture, Sports, Science and Technology grant (#18073013) and the Japan Society for the Promotion of Science grant (#18GS03140013). The funders had no role in study design, data collection and analysis, decision to publish, or preparation of the manuscript.

Competing Interests: The authors have declared that no competing interests exist.

* E-mail: toyama-imhp@umin.ac.jp (TT); kztanabe@biken.osaka-u.ac.jp (KT)

¤ Current address: Department of Dermatology, Course of Integrated Medicine, Graduate School of Medicine, Osaka University, Yamadaoka, Suita, Osaka, Japan

Introduction

Malaria, caused by the genus *Plasmodium*, is one of the most common infections in the world responsible for about 1 million deaths per year. Artemisinin-based combination therapies (ACTs) are currently the first-line and only the best weapon against malaria [1]. Drug resistance, which rendered chloroquine and sulfadoxine-pyrimethamine infective for malaria control from 1970 to 1990s, remains as one of the greatest challenges facing malaria control today. Besides, ACT is 4 to 22× more expensive than common drugs and access is generally poor in African countries [2]. Also, although its clinical efficacy has not yet been compromised, there are recent reports that show the first evidence of artemisinin resistance [3]. Admittedly, the development of new inexpensive, effective and safe drugs with new mechanisms is strongly needed.

Plant-specific organelles and mechanisms in the phylum *Apicomplexa*, in which *Plasmodium* and other medically and veterinarily important pathogens are included, have been brought to focus as potential targets for new drugs since associated enzymes were found in plants and bacteria but not in animal metabolic pathways. Examples of these are plant-like vacuoles in parasite cells and the mevalonate-independent biosynthesis of isoprenoid in apicoplasts [4], [5]. The rationale was further strengthened with the demonstration that the apicoplast is essential for malaria parasite survival [6] and that metabolic pathways in the apicoplast are essential for parasite growth [7]. In addition, identification of inhibitors in these pathways might also result in synergistic drug combinations, which could have increased therapeutic value. The plant hormone abscisic acid (ABA) and ABA biosynthetic inhibitors have, likewise, been shown to affect parasite egress from infected host cells in *Toxoplasma gondii* [8].

In this study, we have preliminarily explored a wide variety of plant growth regulators, including plant hormones and corresponding inhibitors, to investigate their effect(s) on the growth of the most virulent human malaria parasite, *Plasmodium falciparum*. We have also used the apicomplexan parasite, *T. gondii* for comparison. *T. gondii* infects a broad spectrum of hosts and efficient drugs with low side effects and usable for human therapies are also highly needed. Plant growth inhibitors are commonly used in agriculture for years and have been synthesized in bulk, efficiently and cheaply, either naturally or artificially. Well-

established manufacturing methods and facilities, as well as their safety profile (toxicity and teratogenicity) in animals, crops and humans are also available. Thus, plant growth inhibitors showing anti-apicomplexan activities might give valuable clues for prophylactic or therapeutic reagents effective for infectious diseases caused by protozoan parasites.

Materials and Methods

Chemicals

AMO-1618 (2-isopropyl-4-dimethylamino-5-methyl-phenyl-1-piperidinecarboxylate methyl chloride) was obtained from CALBIOCHEM (La Jolla, USA). FC-907 [*N,N,N,*-trimethyl-1-methyl-(2′,6′-trimethylcyclohex-2′-en-1′-yl)prop-2-enylammonium iodide] was kindly provided by Prof. Y. Kamiya (RIKEN, Japan). LysoTracker® Red DND-99 was obtained from Invitrogen (San Diego, USA). All other chemicals were purchased from Wako Pure Chemicals (Osaka, Japan).

Prior to use and dilution at various concentrations, AMO-1618, chlorocholine chloride, prohexadione and FC-907 were dissolved in distilled water. INA and ancymidol were dissolved in DMSO and diluted in 0.1% DMSO. Paclobutrazol and uniconazole P were dissolved in ethanol and diluted in the culture medium.

Enantiomeric resolution of racemic INA (Wako) was carried out by high performance liquid chromatography (HPLC; LC-908, Japan Analytical Industry Co., Ltd, Japan). Elution order of enantiomers was determined by an ultraviolet absorption detector (SPD-10A, Shimadzu, Japan) using Chiralcel OD column [25×0.46 cm, Daicel Chemical Industries, Japan, mobile phase: n-hexane-2-propanol (7:3, v/v), flow rate: 1.0 ml/min]. All resolutions were carried out at 26°C; detection at 275 nm. The assignment of the peaks was achieved by comparison with the synthesized (*S*)-form INA sample as previously described [9]: peak with shorter retention time correspond to the (*R*)-form and the peak with longer retention time to the (*S*)-form. Percentage purity of the products was calculated to be 97.0% and 99.5% for (*S*)- and (*R*)-forms, respectively, based on peak areas.

In vitro culture

P. falciparum strain 3D7 was cultured at 3% hematocrit in RPMI 1640 supplemented with 10% human serum, 50 mg/l hypoxanthine and 25 mg/l gentamicin, as previously described [10]. Cultures were maintained at 37°C in a gas mixture of 5% CO_2, 5% O_2, and 90% N_2.

The *T. gondii* strain 2F tachyzoites, derived from strain RH, constitutively expressing cytoplasmic β-galactosidase (β-gal), were routinely grown in Vero cells (African green monkey kidney, strain ATCC CCL-81^{TM}) at 37°C under 5% CO_2 in RPMI 1640 medium containing 10% fetal calf serum [11].

In vitro antimalarial assay of plant growth regulators

Asynchronous *P. falciparum* 3D7 was used. Various concentrations of compounds in appropriate solvents (water, ethanol or DMSO) were prepared and added to 12-well plates. Starting parasitemia was at 0.1% in 2.5 ml culture medium. Growth was assessed after 72 h by percentage parasitemia using thin blood smears. The number of parasitized erythrocytes over a total of 3,000 erythrocytes was examined. Drug-free control cultures were run simultaneously.

For *T. gondii* studies, confluent Vero cell cultures were incubated for 2 days and infected with 2.5×10^5 tachyzoites in RPMI 1640 medium containing 3% FCS using a 96-well plate. Tachyzoites were harvested after 2 days and β-gal activity was analyzed using a colorimetric assay [12].

Morphological effects of gibberellin biosynthetic inhibitors on P. falciparum

Tightly synchronized parasites within 4 h life span were prepared using 5% sorbitol treatment and percoll centrifugation. Synchronized parasites were treated with either 50 μM INA or 250 μM AMO-1618 from 0 h (ring), 20 h (immature trophozoite), 28 h (mature trophozoite) or 36 h (schizont). Giemsa-stained thin-blood smears were prepared after 4, 8 and 12 h treatment. Digital imaging was performed on a HC-300 (Fujifilm, Japan) and representative parasite images are shown.

Fluorescence Microscopy

Thin-blood smears of infected erythrocytes treated with INA were stained with acridine orange (100 μg/ml). Fluorescence microscopy and confocal imaging were carried out using the Axioplan 2 microscope (Zeiss, German) and SPOT PS-BW CCD camera (Seki Technotron Corp., Japan). Filter sets for green fluorescence (green: nucleoli; emission LP515, excitation BP 450–490) and red fluorescence (red: cytoplasm; emission LP590, excitation 546/12) were used. Nile Red staining was carried out by addition of 1 μg/ml dye to the culture medium 1 h prior to microscopic analysis. Nile Red was excited at 546 nm and emission detected above 590 nm. To stain with rhodamine 123 and LysoTracker® Red DND-99, 10 ng/ml rhodamine or 75 nM LysoTracker were added to the culture and incubated for 1 h. Confocal images were obtained with excitation above 546 nm and emission above 590 nm.

Electron microscopy

Intraerythrocytic parasites treated with 50 μM INA for 6 h, 250 μM AMO-1618 for 8 h or 0.1% DMSO for 6 h were centrifuged at 3500× g for 1 min and fixed in 2% glutaraldehyde in 1× PBS for 1 h. After washing in 1× PBS, fixed cells were treated as described [13]. Sections were viewed in a transmission electron microscope JEM-1011 (JEOL Ltd., Japan).

Effects of osmotic pressure on INA-treated P. falciparum

P. falciparum in RPMI 1640 containing 10% human serum was grown to 5–10% parasitemia and synchronized by sorbitol treatment. After 21 h, 0.9 ml of early trophozoite-stage parasites was mixed with 0.1 ml of 1×, 2×, 3× and 4× PBS and treated simultaneously with 50 μM INA or 0.1% DMSO for 8 h (INA stock solution was prepared as 50 mM in DMSO and diluted to 1/1000 for assay). Parasitemia was determined using Giemsa-stained thin smears by a laboratory technician blinded to treatment assignments. Each treatment was replicated thrice and experiments were performed twice.

Volumes of 0, 0.1, 0.2 and 0.4 ml sterilized water was adjusted to 0.4 ml by mixing with appropriate amounts of RPMI 1640 medium containing 10% human serum for the different dilution series. Hyposmotic media were mixed with 0.6 ml of *P. falciparum* culture synchronized to early-stage trophozoites.

GC-MS analysis of sterols in P. falciparum

Parasites were cultured in 5 ml RPMI 1640 supplemented with 1% serum free AlbuMAX® II (Invitrogen). Parasitized erythrocytes were collected by centrifugation and hemolyzed in 0.54 ml of 0.15% saponin in RPMI 1640. Erythrocyte-free parasites were washed twice with 4 ml of 1× PBS and suspended in 0.4 ml of 1× PBS. Geranylgeraniol at 50 μg was added to the suspension as an internal standard and extraction with 1 ml of chloroform was carried out 3 times by shaking the mixture at 37°C.

Chloroform extracts were pooled and 1 µl solution was directly injected into the GC-MS (gas chromatography/mass spectroscopy) instrument (JEOL; JMS-Bu25 GCMate: ionization energy at 70 eV, filament current at 300 mA) with a DB-5 capillary column [0.25 mm i.d.×15 m, film thickness of 0.25 mm (J&W Scientific, USA)]. The He carrier gas flow rate was 1 ml/min (constant flow), the injector temperature was 250°C, and the samples were introduced by splitless injection. After injection, the oven temperature program was held at 80°C for 1 min, then increased to 200°C at 30°C min^{-1}, followed by a further increase to 300°C at 15°C min^{-1} after which it was held constant at 300°C for 2 min.

For quantitative analysis, commercially available cholesterol and geranylgeraniol (Sigma) was detected by GC-MS and corresponding peaks were used as authentic standards for cholesterol and geranylgeraniol, respectively. Cholesterol was calculated based on ratio of peak areas with geranylgeraniol.

Results

Antimalarial activity of gibberellin biosynthetic inhibitors

All inhibitors of gibberellin used in this study affect synthesis of gibberellin in plants (Fig. 1). Generally, the inhibitors blocked *P. falciparum* growth *in vitro* (Table 1, Fig. S1); although, results were admittedly different among the inhibitors as well as between *Plasmodium* and *Toxoplasma*. For example, inabenfide (INA) exerted strong activities in both *P. falciparum* and *T. gondii*, whereas prohexadione exhibited no cytotoxicity to *P. falciparum* even at 500 µM. Likewise, ED_{50}s of some inhibitors varied greatly between *P. falciparum* and *T. gondii*, such as AMO-1618: 10.3±2.22 µM in *P. falciparum* and >1000 µM in *T. gondii*. Apparent difference in effective inhibitor concentrations between the two parasite species could be species-specific barrier on membranes for drug uptake or inhibitory mechanisms in *P. falciparum* and *T. gondii* [14].

Some of the tested inhibitors have an asymmetric carbon, and their enantiomers are known to differ significantly in their biological properties [15]. (*S*)-forms are biologically more active than (*R*)-forms in higher plants [16]. In order to examine the chirality effect of these inhibitors, we separated enantiomers from commercially available INA by HPLC using a chiral column (Fig. S2) since marketed INA is racemic. The (*S*)-form was slightly more potent than the (*R*)-form, as demonstrated by ED_{50} values of 2.78±0.51 µM and 6.32±0.81 µM, respectively in *P. falciparum* (Table 1). Notably, the (*R*)-form was more effective in inhibiting growth of *T. gondii*.

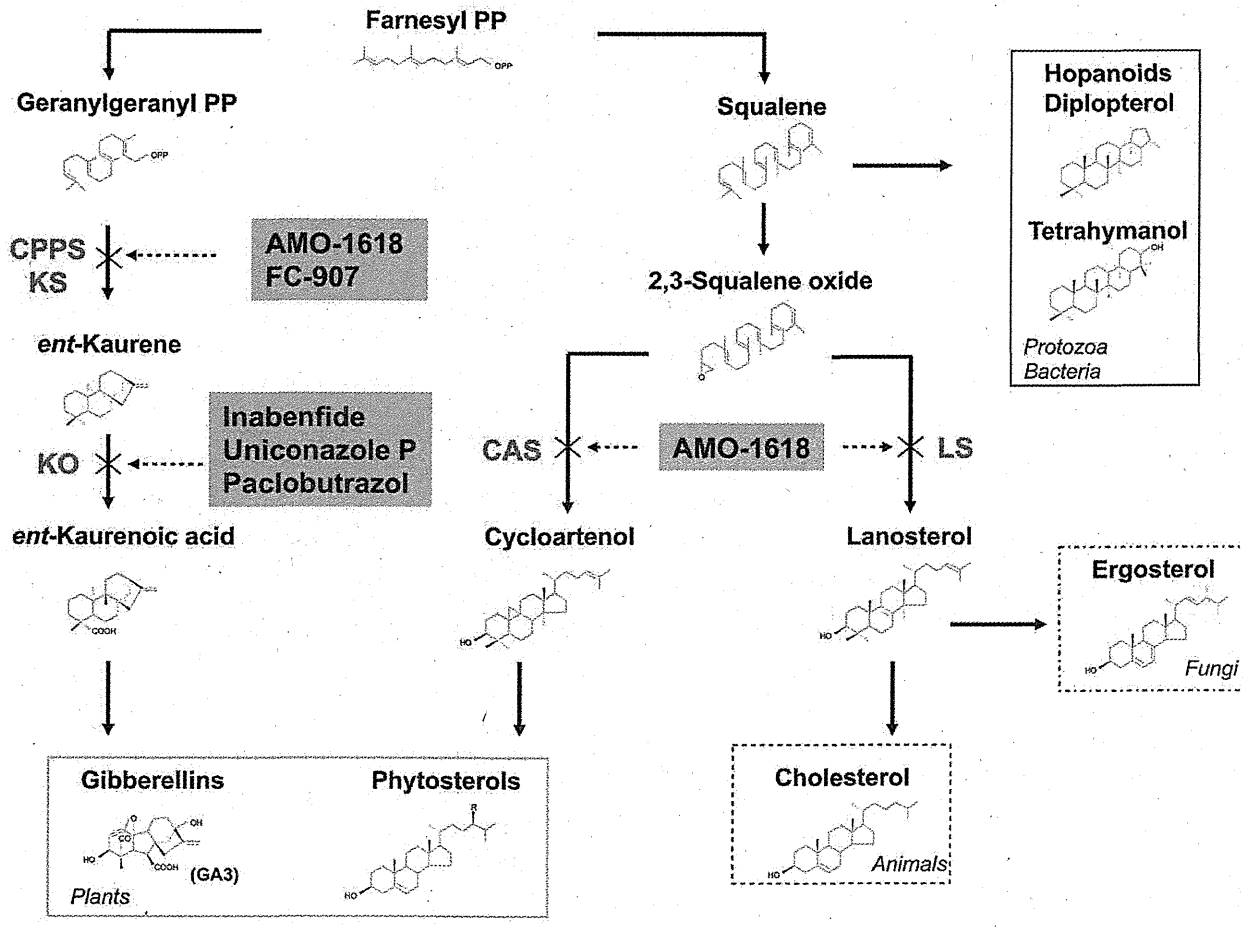

Figure 1. Isoprenoid biosynthetic pathways and known inhibitors in various organisms. Broken arrows indicate blocks in the biosynthesis due to specific inhibitors. "R" indicates various functional groups specific to individual compounds. CPPS, copalyl-diphosphate synthase (EC 5.5.1.13); KO, *ent*-kaurene oxidase (EC 1.14.13.78); CAS, cycloartenol synthase (EC 5.4.99.8); LS, lanosterol synthase (EC 5.4.99.7); KS, *ent*-kaurene synthase (EC 4.2.3.19); PP, pyrophosphate.
doi:10.1371/journal.pone.0032246.g001

Table 1. ED_{50} of the gibberellin biosynthetic inhibitors.

Reagents	ED_{50} of *P. falciparum* (μM)	ED_{50} of *T. gondii* (μM)
Chlorocholine Chloride	8.94±26.08	>10000
AMO-1618	10.3±2.22	>1000
FC-907	4.26±0.14	2206.7±2.46
Inabenfide	2.94±0.15	17.0±1.32
Paclobutrazol	27.1±2.69	120.6±5.38
Uniconazole P	30.7±6.20	97.4±8.66
Ancymidol	322.9±13.1	>1000
Prohexadione	>500	>10000
(*S*)-Inabenfide	2.78±0.51	24.04±1.07
(*R*)-Inabenfide	6.32±0.81	6.23±1.65

Growth inhibitory effects of gibberellin biosynthetic inhibitors and enantiomers of INA to *P. falciparum* and *T. gondii* are shown. Values are the mean ± standard deviations (SD) from three independent experiments, with each treatment duplicated twice. N.D.; not determined.
doi:10.1371/journal.pone.0032246.t001

Morphological changes induced by gibberellin biosynthetic inhibitors

We also evaluated morphological and physiological effects induced by the gibberellin biosynthetic inhibitors. In what appears to be the center of the parasite, a Giemsa-unstained region was prominent within 4 h after treatment with INA (Fig. 2 B). The "haloed" parasites swelled and ruptured within 12 h of culture in immature trophozoite-stage. Rings were seldom found when early trophozoite-stage parasites were treated with INA. When INA was applied at late stages of the parasite, *i.e.* in mature trophozoites and schizonts, a similar swelling was also observed although the stained periphery appears broader with merozoites bloated in appearance and few in number (Fig. 2 C, D). Ring-stage treated parasite cultures were usually appliqué forms (rings appearing on the periphery of the erythrocytes) (Fig. 2 A).

Another type of gibberellin biosynthetic inhibitors, AMO-1618 and FC-907, which prevent cyclization reaction in the early steps of gibberellin biosynthesis (Fig. 1) [15], [17], also caused parasite cells to swell. Swelled parasites were found within 8 h and 24 h after AMO-1618 treatment (Fig. 2, S3), but the altered morphology on schizonts was different: parasites appear abnormally disordered inside erythrocytes (Fig. 2 C, D). A similar morphological change in *Plasmodium* cultures were observed when greater than 2 μM INA were used (data not shown). Notably, both INA and AMO-1618 did not appear to damage erythrocytes, because *P. falciparum* could infect erythrocytes that had been treated for 24 h with 50 μM INA or 250 μM AMO-1618 without any significant inhibitory effects (Fig. S4).

At 2 μM, INA-induced morphological changes were microscopically visible at 24 h in asynchronous parasite cultures. In order to determine if INA and AMO-1618 targets a specific stage during intraerythrocytic development, we increased concentrations of INA to 50 μM and AMO-1618 to 250 μM. Both inhibitors at these concentrations provoked morphological changes more rapidly than concentrations at their ED_{50}s (Fig. S5). The use of increased concentrations of inhibitors also allowed us to measure the intrinsic sensitivity of the parasites *in vitro*, and provided clues to the maximal response that can be produced by these inhibitors, as well as their toxicity to the human erythrocytes. Even after 24 h incubation, use of 0.1% DMSO alone gave no effects on growth and morphology of malaria parasites. Parasite swelling and rupture was also observed on *P. falciparum* cultures treated with other gibberellin biosynthetic inhibitors, such as paclobutrazol and uniconazole P (Fig. S5). These inhibitors, as well as INA, are known to block cytochrome P450-dependent monooxygenases (CYP701A) in plants [15]. Interestingly, the time and the concentrations necessary to provoke morphological changes were different among these compounds, presumably due to differences in solubility and lipophilicity.

The 'haloed' trophozoites

The "haloed" parasites were stained with various fluorescent probes to visualize intracellular components. The center of the trophozoites was not stained with acridine orange (Fig. 3 A). Both nuclei and cytoplasm appear to be on the periphery, as seen in the Giemsa-stained images. Nile Red, used to visualize various lipid-rich compartments such as membranes, endoplasmic reticulum (ER) and lipid bodies [18], revealed a simpler staining pattern surrounding what appears to be fewer merozoites in contrast to the control. Merozoites also appear bloated with intense spots of fluorescence (presumed as lipid bodies, Fig. 3 B). In normal mature stage trophozoites, rhodamine 123 showed thread-like branched mitochondria, characteristic of the mitochondrial development at the later stages where each daughter merozoite receives a branch of the parent organelle (Fig. 3 C) [19]. In INA-treated parasites, however, branched mitochondria were rarely seen. Although fluorescence intensity in the mitochondria started to decrease after 2 h, parasites still have significant fluorescence over the entire parasite cytosol, except in the food vacuole, similar to untreated parasite cells. This observation suggest a membrane potential generated by the parasite's outer plasma membrane [20], [21] and that INA effect likely induced a specific reduction in the mitochondrial membrane potential alone.

These differences in the staining patterns were not evident when ring-stage parasites were observed (data not shown), which suggest that various membranes were remarkably affected by INA only when parasites reached the trophozoite stage. The timing is coincident at a time when the parasite starts to actively generate membranes needed for growth and schizogony [22].

Electron microscopy also revealed fine intracellular differences at the trophozoite and schizont-stage parasite (Fig. 4 A, B). When trophozoites were treated with INA or AMO-1618 (Fig. 4 A), membranes of the nuclear envelope and ER were thicker and intensely stained compared to control parasites. Conspicuously unfamiliar spaces appeared around the ER and daughter nuclei (Fig. 4 A, INA and AMO-1618 panel). Using asynchronous cultures, these spaces were more readily observed at mature-stage parasites than early trophozoites (Fig. 4 B, b and f vs. c and d). No differences were evident in the plasma membranes of both host and parasite cells during the intraerythrocytic life cycle (Fig. 4 B). These results suggest that the gibberellin biosynthetic inhibitors appear to affect components of various intracellular membranes of the parasites, and the effects were especially evident during schizogony.

INA effect and osmotic pressure in parasite cells

Various stressful conditions were applied to INA treated parasite: use of hydraulic pressure, ultrasound, pH (5–9) and temperature changes (4–37°C); but no differences were observed when compared to control parasites (DMSO-treated). However, different responses were seen when trophozoite-stage parasites were under various osmotic stress. Hyperosmotic conditions were achieved by incubating with 10% (v/v) 1×, 2×, 3× or 4× PBS. For control, untreated parasite cultures, relative parasitemia drastically decreased with increasing hyperosmotic environment (Fig. 5 A). However, relative parasitemia in the INA-treated

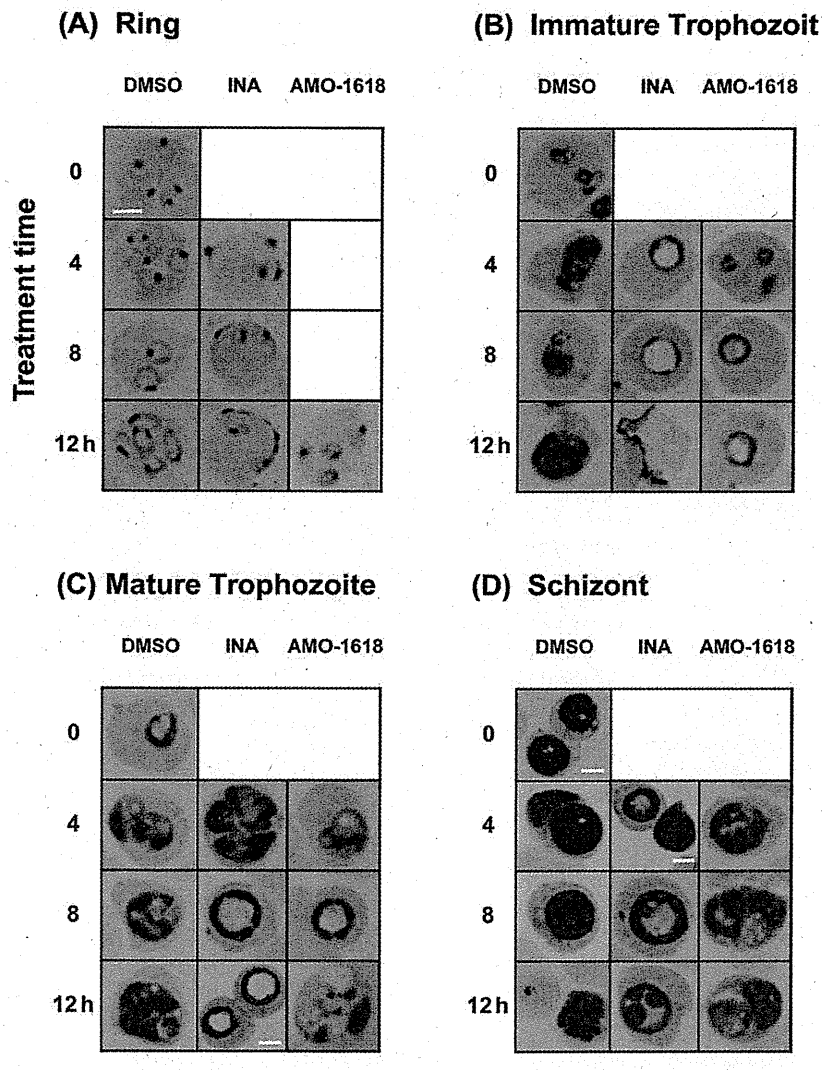

Figure 2. Effect of INA and AMO-1618 on intraerythrocytic development of *P. falciparum*. Tightly synchronized parasite cells that have undergone 5% sorbitol treatment and percoll density gradient centrifugation (window period: 4 h) were treated with 1 μl/ml DMSO, 50 μM INA or 250 μM AMO-1618 at different parasite stages: after 0 h (ring, A), 20 h (immature trophozoite, B), 28 h (mature trophozoite, C) and 36 h (schizont, D). Cultures were examined after 4, 8 and 12 h using Giemsa thin blood smears. Scale bar: 3 μm; all images without a scale bar are displayed at the same scale as the left uppermost image in (A).
doi:10.1371/journal.pone.0032246.g002

samples increased in higher hyperosmotic environment, especially in cultures treated with 10% 4× PBS. Moreover, 'haloed' trophozoites were less evident in cultures incubated with 3× or 4× PBS. To examine the potential effects of cation species, we made a solution where the net solute was the same to PBS but the concentrations of Na^+ and K^+ were reversed (137 mM KCl, 8.1 mM K_2HPO_4, 2.68 mM NaCl, and 1.47 mM NaH_2PO_4). Between normal and reversed PBS in the different treatments, no significant differences were observed in both parasitemia and morphology (Fig. S6). Exogenously added Ca^{2+} (100 μM) to cultures did not help reverse the 'haloed' effects of INA in trophozoites (Fig. S7).

Hyposmotic stress enhanced INA's effect in treated parasites: early trophozoite-stage parasites swelled even more by the addition of 10% (v/v) water to the culture medium (Fig. 5 B). At 40% (v/v) water, trophozoites swelled to almost the same volume of the infected erythrocyte. Decrease in parasitemia was also statistically significant compared to the control. These observations suggest that INA treatment might affect membrane permeability; water or ion influx might cause swelling of the parasites.

Isoprenoid biosynthetic pathway in apicomplexan parasites

Parasite cultures were incubated with gibberellin A_3 and A_4, the most effective gibberellins, with or without gibberellin biosynthetic inhibitors. Of note, gibberellins did not affect growth of parasites nor overcome the effects of the inhibitors (data not shown), suggesting that the inhibitors could not disrupt gibberellin biosynthesis in *P. falciparum* or malaria parasites do not utilize gibberellins.

Gibberellins are diterpene (isoprenoid), ubiquitous and essential compounds by themselves or as materials of secondary metabolites

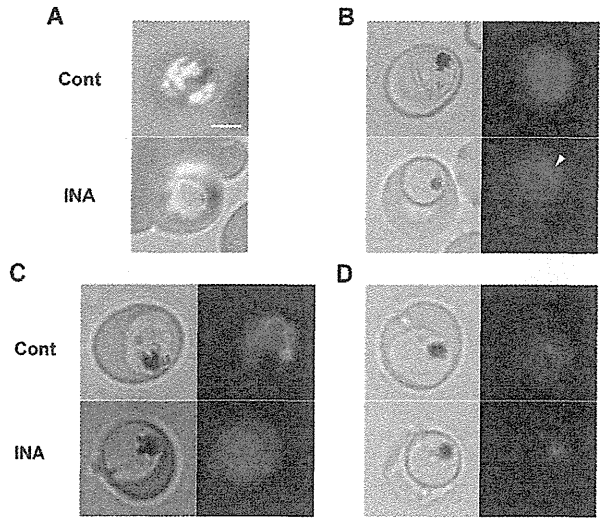

Figure 3. Fluorescence microscopy of INA-treated parasites. Infected erythrocytes were stained with (A) acridine orange, (B) Nile Red, (C) rhodamine 123 and (D) LysoTracker™ Red DND-99. INA was introduced at: (A) 100 μM for 9 h, (B) 50 μM for 6 h, and (C and D) 50 μM for 4 h. 100 μg/ml acridine orange was applied to thin blood smears made from intraerythrocytic parasites treated with INA. For other fluorescence dyes, *P. falciparum* cultures were incubated with probes for 1 h at the following concentrations: Nile Red, 1 μg/ml; rhodamine 123, 10 ng/ml; and LysoTracker® Red DND-99, 75 nM. Cells were not washed prior to fluorescence microscopy to minimize damage due to osmotic changes. Scale bar, 3 μm. An arrow indicates a lipid body in (B).
doi:10.1371/journal.pone.0032246.g003

and signal molecules in animals, plant and bacteria [15]. Biosynthetic pathways of isoprenoids are very complicated and parallel pathways for the biosynthesis of the universal 5-carbon building block for all terpenoid compounds exist. A huge variety of sterols and terpenoids are synthesized via isoprenoid metabolic pathways in a species-specific manner, although all pathways utilize farnesyl pyrophosphate as a starting molecule generated in the mevalonate pathway and the 2-*C*-methyl-D-erythritol 4-phosphate (MEP) pathway (Fig. 1) [23]. Gibberellin biosynthetic inhibitors have been known to block other enzymes leading to the production of sterols and terpenoids. We then analyzed *P. falciparum* treated with INA and AMO-1618 by GC-MS. Interestingly, any sterols or terpenoids besides cholesterol derived from human erythrocytes were not detected, and there were no significant differences in the level of cholesterol between control and INA- or AMO-1618-treated samples (Fig. 6).

Discussion

Efforts on malaria control have been complicated by emergence of drug resistance. With the apicoplast considered to originate from an ancestor with an endosymbiotic alga, and that many non-photosynthetic processes are shared peculiarly with plants, plant growth regulators are of particular interest for pharmaceutical leads on the assumption that the molecular target may not be present in humans. The present study clearly showed some inhibitors that antagonize gibberellin biosynthesis in plants are effective to both *P. falciparum* and *T. gondii* (Table 1). Gibberellin is one of 5 major plant hormones known to exert various effects on physiological events, particularly germination and seed bearing by promoting cell elongation [24]. 126 different gibberellins are known to occur in plants [15], and they are synthesized via the mevalonate pathway and the MEP pathway. Interestingly, gibberellin has been utilized to induce development of parthenocarpous fruits in some fruits such as grapes. On the other hand, gibberellin inhibitors have also been widely used for agriculture, *e.g.* for dwarf plants without harmful effects to either plants or animals.

All gibberellin inhibitors tested in this study block biosynthesis of gibberellin in plants: AMO-1618 and FC-907 block synthesis of *ent*-kaurene (an intermediate during the synthesis of gibberellin) by inhibition of copalyl-diphosphate synthase (CPPS) and *ent*-kaurene synthase (KS, Fig. 1) [15]. Next to AMO-1618 and FC-907 steps, INA, paclobutrazol, uniconazole P and ancymidol interrupt *ent*-kaurene oxidase (KO), a member of the cytochrome P450 monooxygenases (CYP) oxidating *ent*-kaurene into *ent*-kaurenoic acid. Azole antifungal such as fluconazole and diniconazole are analogous compounds to these inhibitors and interrupt synthesis of ergosterol [25]. They have an asymmetric carbon and their enantiomers are known to differ significantly in their biological properties [16], [26]. (*R*)-forms demonstrate stronger activity than (*S*)-forms in terms of fungicidal effects, whereas the latter is functionally active and the (*R*)-forms showed only residual activity with regard to blockage in plant gibberellin biosynthesis. We tested the stereochemical selectivity of INA and found that the (*S*)-form inhibited growth of *P. falciparum* >2 times stronger than (*R*)-form but *vice versa* in *T. gondii* (Table 1). The stereochemical discrimination was, thus, similar to plants than to fungi in *P. falciparum*, although the (*S*)-form was reportedly 1000 times more potent than (*R*)-form in growth retardation of pumpkin seedlings [26]. Differences may be due to discrepancies in protein structures that relate to membrane permeability or translocation of the enantiomers to the site of biosynthesis in such distant species.

The observed decrease in parasitemia in INA-treated cultures correlated with remarkable morphological changes: swelling and rupture of *P. falciparum* cells, particularly when drug treatment commenced during early trophozoite stage (Fig. 2). Trophozoite-stage parasite cells appear to be 'haloed', the center of the cell remains unstained by Giemsa and acridine orange. Both nuclei and cytoplasm were seen on the periphery of the parasite cells. These data suggest that some substances that are neither acidic nor alkaline might accumulate in the unstained parts.

We also observed the intracellular structures in INA-treated cultures using different dyes and found that various intracellular organelles, especially organelles synthesized during schizogony (such as mitochondria, membrane network and food vacuoles) are morphologically abnormal or compromised after short treatment with INA (Fig. 3). Membrane potential in the mitochondria was reduced rapidly within 2 h of INA treatment. Organelle membranes such as those in the ER and nuclear envelope appeared thicker and gaps were observed around such organelles under electron microscopy (Fig. 4). From these observations, it appears that gibberellin biosynthetic inhibitors damage the parasite internal organelles, compromises parasite membranes and results to abnormalities in the treated parasites.

In order to further probe for clues that can shed light into the mechanisms for such changes in the membranes, we exposed INA-treated parasite cells to various stresses, and found that osmotic pressure modified the effects of INA. Treated parasite cells under hyperosmotic conditions became less swelled and viability was significantly restored (Fig. 5 A). In contrast, the addition of water in the culture medium enhanced expansion and rupture of parasites (Fig. 5 B). These results demonstrate that INA treatment might affect permeability of membranes, and consequently result to uncontrollable influx of water or ion into parasite cells. No abnormalities in the plasma membrane structure were observed by electron microscopy (Fig. 4), although this cannot be completely ruled out since parasites with severely compromised plasma

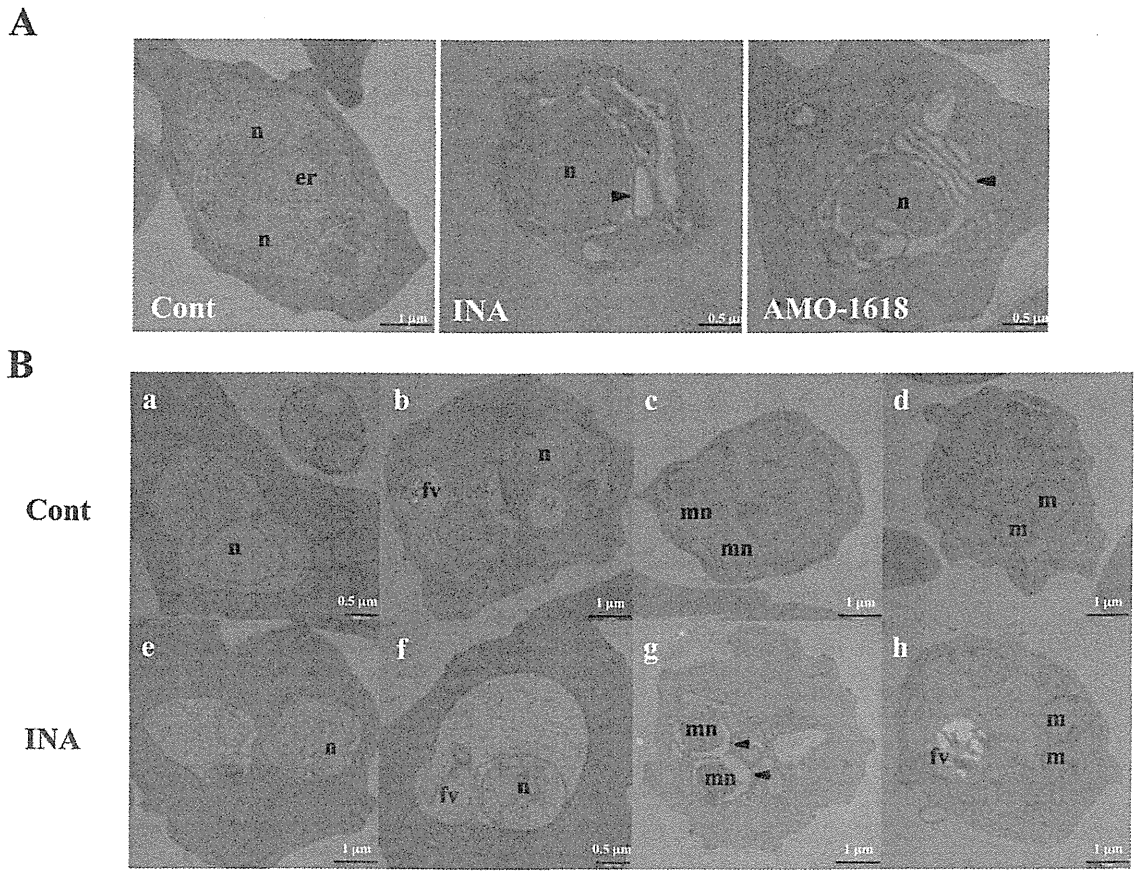

Figure 4. Transmission electron microscopy of parasitized erythrocytes treated with inhibitors. (A) Sections through an erythrocyte containing a trophozoite-stage parasite exposed to 0.1% DMSO for 6 h, 50 μM INA for 6 h or 250 μM AMO-1618 for 8 h, respectively. (B) Asynchronized parasites were treated with 0.1% DMSO (a–d) or 50 μM INA for 6 h (e–h). Sections from representative stages during intraerythrocytic development: ring- (a and e), early trophozoite- (b and f), mature trophozoite- (c and g) and schizont-stage parasites (d and h) are shown. Nuclei (n), food vacuoles (fv), merozoites (m), nuclei of merozoites (mn) and abnormal gaps between the nuclei and the nuclear envelopes (arrowheads) are indicated. Scale bar is indicated at the bottom of the images.
doi:10.1371/journal.pone.0032246.g004

membranes are very likely susceptible to rupture or bursting during various treatments for microscopy.

In order to maintain the various functions and stability of plasma membranes, different organisms synthesize several specific components for their biological membranes. For example, sterols, a vast family of isoprenoids, take pivotal role with mammalian and fungal cells generally synthesizing one major sterol, cholesterol and ergosterol, respectively [23], [27]. Plants, on the other hand, are known to produce a characteristically complex sterol mixture. As many as 61 sterols and isoprenoids have been identified in a single maize seedling [28]. Prokaryotes produce hopanoids, pentacyclic isoprenoids, by direct cyclization of squalene (Fig. 1) [29]. The functions of the hopanoids were shown to be equivalent to sterols: functioning as membrane reinforcers affecting membrane permeability and fluidity. In protozoa, there has been one report that *Tetrahymena* synthesizes tetrahymanol, a quasi-hopanoid, together with small amounts of diplopterol [30], [31]. Both components were incorporated into its membranes.

Enzymes that are involved in gibberellin biosynthesis are also of importance in the formation of such sterols and other membrane constituents. Change in the level of these substances after treatment with inhibitors has been often observed as side activities for these inhibitors [15]. For example, AMO-1618 inhibits syntheses of phytosterols and cholesterol, by blocking cycloartenol synthase (CAS) in plants and lanosterol synthase (LS) in animals, respectively [32].

We analyzed *P. falciparum* treated with INA and AMO-1618 by GC-MS in order to identify sterols or isoprenoids in malaria parasites, but we could not detect any isoprenoids, besides cholesterol (Fig. 6). We might be able to hypothesize that responsible components could be too low or structurally unknown to detect by GC-MS in parasite cells. Data about syntheses of isoprenoids in protozoa, especially in *Apicomplexa*, remains nil. Intraerythrocytic parasites are known to intake large amounts of erythrocyte contents with surrounding membranes that are cholesterol rich, however, cholesterol is greatly depleted in parasite membranes (Fig. 6 A) [33]. How parasites transport and dispose of excess cholesterol within the cells remain a puzzle. Additionally, does lack of isoprenoids make membranes leaky even in intracellular parasites? A previous study has demonstrated by differential scanning calorimetry and electron spin resonance the association of gibberellin molecules with phospholipid membranes thereby altering the fluidity or viscosity of the lipid bilayer [34]. Clearly, further studies on gibberellin biosynthetic inhibitors could shed light if these compounds could perturb lipid bilayers or alter properties of the membrane phospholipid.

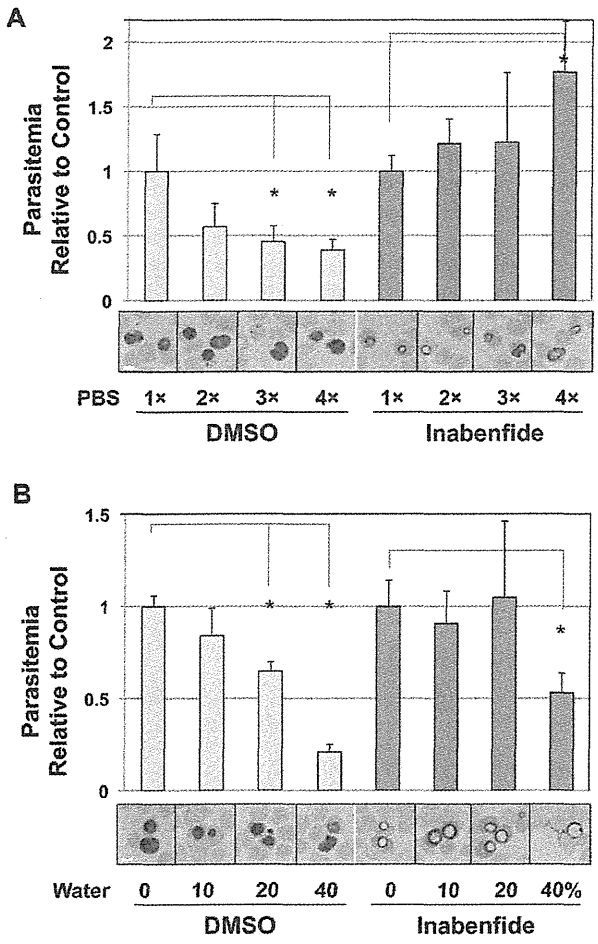

Figure 5. Effects of osmotic pressure to intraerythrocytic parasites treated with INA. (A) Effects of hyperosmotic stress in INA-treated parasites. *P. falciparum* cultures treated with 50 μM INA were observed in various dilution ratios of PBS for 8 h. Parasitemia was determined by Giemsa-stained thin blood smears. Student's *t*-test: *P>0.005. Values are means ± SD of n=6 in two independent experiments. Data were normalized relative to control cultures (1× PBS) in DMSO- and INA-treated samples, respectively. Representative parasite morphologies are shown for each treatment. Scale bar, 3 μm. (B) Effects of hyposmotic stress, experimentally induced by the addition of water to the culture medium of *P. falciparum*, after 8 h of 50 μM INA treatment. N=6 smears each in two independent experiments.
doi:10.1371/journal.pone.0032246.g005

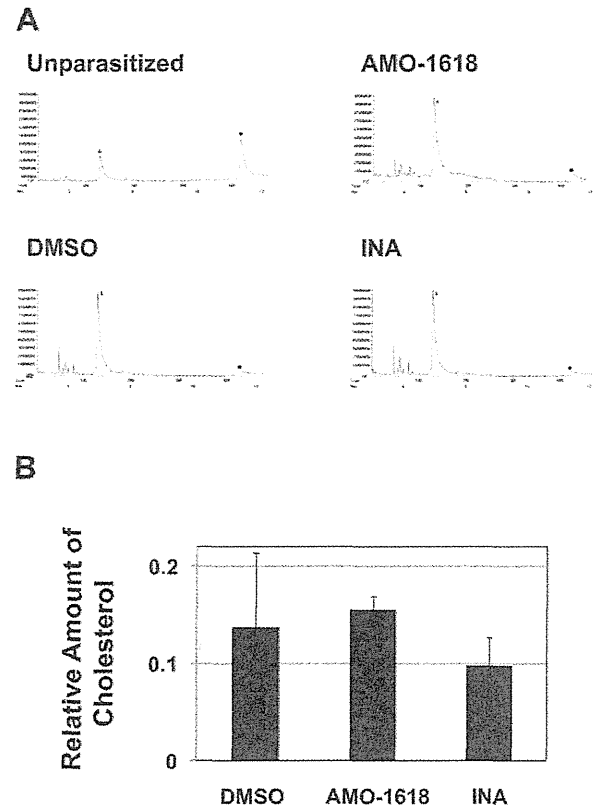

Figure 6. GC-MS analysis of isoprenoids in *P. falciparum in vitro* cultures. (A) Total ion chromatograms of extracts from unparasitized erythrocytes (Unparasitized), parasites treated with 0.1% DMSO, 250 μM AMO-1618, and 50 μM INA for 6 h. Triangles and circles indicate the peaks of geranylgeraniol mixed as an internal control (retention time=6.57 min) and cholesterol (11.23 min), respectively. These compounds were identified by direct comparison with authentic samples. (B) Quantification of cholesterol in each treated sample. Cholesterol amount was calculated from the peak areas and normalized relative to the ratio of the internal control geranylgeraniol. Values are means and SD of triplicate measurements of a representative experiment.
doi:10.1371/journal.pone.0032246.g006

The gibberellin biosynthetic inhibitors are known to be specific for isoprenoid biosynthesis in plants. We searched amino acid sequences and conserved domain sequences essential for these enzymes using PlasmoDB, but no sequences with significant homologies were found. This may imply the uniqueness of isoprenoid metabolic pathways in *Apicomplexa*, and consequently, provide potent targets to develop novel therapeutic agents.

Supporting Information

Figure S1 Concentration-response curve of INA. Each point represents the mean ± standard deviations (SD) from three independent experiments, with each treatment duplicated twice.
(TIF)

Figure S2 Chiral separation of enantiomeric INA. Racemic form of INA was separated on Chiralcel OD column. Mobile phase: n-hexane-2-propanol (8:2, v/v), flow rate:10 ml/min, detection: 275 nm. HPLC chromatograms of each enantiomer are also shown.
(TIF)

Figure S3 Effect of gibberellin biosynthetic inhibitors on the intraerythrocytic development of *P. falciparum*. Asynchronized parasites were treated with 200 μM FC-907 for 24 h, 500 μM uniconazole P for 8 h, 200 μM paclobutrazol for 8 h, 50 μM INA or 1 μl/ml DMSO for 6 h. Giemsa-stained thin blood smears were prepared from each sample after the indicated treatment and examined under a microscope. Each panel shows the typical morphology of trophozoite-stage parasites in each treatment. Scale bar, 3 μm.
(TIF)

Figure S4 Effects of gibberellin biosynthetic inhibitors on the viability of erythrocytes to support growth of *P. falciparum*. Erythrocytes that had been incubated in RPMI

1640 containing 10% human serum and supplemented with 1 µl/ml DMSO, 50 µM INA or 250 µM AMO-1618 for 24 h were washed with RPMI 1640 twice and mixed with *P. falciparum* infected erythrocytes at 0.3% starting parasitemia. Thin blood films from each culture were prepared after 48 h, stained with Giemsa and parasitemias were counted under a microscope. Values are mean ± SD of n = 3 in each representative experiment.
(TIF)

Figure S5 Influence of INA concentration on growth inhibition in *P. falciparum*. (A) Synchronized parasites at early trophozoite stage were treated with 0 (1 µl/ml DMSO), 10 or 50 µM INA for 0–8 h. Parasitemia was determined by thin blood films after staining with Giemsa. Error bars represent the standard deviation (SD) of three independent experiments made in duplicate. Data are normalized relative to those for the control treated for 0 h. (B) The parasites treated with 0, 10 or 50 µM INA after 4 h, stained with Giemsa, and visualized under light microscope. Scale bar = 3 µm. Each panel shows the typical morphology of trophozoite-stage parasites in each treatment.
(TIF)

Figure S6 Effects of cation species to the parasitemia of the intraerythrocytic parasites treated with INA. Synchronized parasites at early trophozoite stage were mixed with 10% of 1× and 4× normal PBS or the solution that Na^+ and K^+ concentrations in PBS are exchanged (reversed-PBS; 1× reversed-PBS contains 137 mM KCl, 8.1 mM K_2HPO_4, 2.68 mM NaCl, 1.47 mM NaH_2PO_4), and treated with 50 µM INA or 1 µl/ml DMSO for 8 h. Parasitemia was determined by counting thin blood film from each culture blindly after staining with Giemsa; the counter was blinded to sample identities. Error bars represent the standard deviation of three independent experiments made in duplicate. Data are normalized relative to those for the control treated with 1× PBS and 1 µl/ml DMSO.
(TIF)

Figure S7 Influence of Ca^{2+} on the effects of INA in *P. falciparum*. Parasites were synchronized by 5% sorbitol treatment and treated with 1 µl/ml DMSO or 50 µM INA with or without adding 100 µM $CaCl_2$ after 18 h of incubation. The parasites were examined at 6 h of the treatment by thin blood smears and staining with Giemsa. Scale bar indicates 3 µm. Each panel shows a typical morphology of trophozoite-stage parasites in each treatment.
(TIF)

Acknowledgments

The authors greatly appreciate Prof. Yuji Kamiya (RIKEN, Japan) for kindly providing FC-907. We are deeply grateful to Dr. Eri Hayakawa (Tokyo Women's Medical University, Japan) for technical advice, Hiroko Omori (Osaka University, Japan) for expert work in transmission electron microscopy, Yohei Ueno (Graduate school of agriculture, TUAT, Japan) for GC-MS, and Sawako Itagaki and Mayumi Fukui (Osaka University, Japan) for culturing and counting parasitemia.

Author Contributions

Conceived and designed the experiments: TT KN NMQP HK TH KT. Performed the experiments: TT MT KN HK. Analyzed the data: TT MT KN HK. Contributed reagents/materials/analysis tools: KA YH. Wrote the paper: TT KN KA NMQP HK KT.

References

1. Eastman RT, Fidock DA (2009) Artemisinin-based combination therapies: a vital tool in efforts to eliminate malaria. Nat Rev Microbiol 7: 864–874.
2. Adeyi O, Atun R (2010) Universal access to malaria medicines: innovation in financing and delivery. Lancet 376: 1869–1871.
3. Noedl H, Se Y, Schaecher K, Smith BL, Socheat D, et al. (2008) Evidence of artemisinin-resistant malaria in Western Cambodia. N Engl J Med 361: 2619–2620.
4. Miranda K, Pace DA, Cintron R, Rodrigues JCF, Fang J, et al. (2010) Characterization of a novel organelle in *Toxoplasma gondii* with similar composition and function to the plant vacuole. Mol Microbiol 76: 1358–1375.
5. Wiesner J, Borrmann S, Jomaa H (2003) Fosmidomycin for the treatment of malaria. Parasitol Res 90: S71–S76.
6. Fichera ME, Roos DS (1997) A plastid organelle as a drug target in apicomplexan parasites. Nature 390: 407–409.
7. Jomaa H, Wiesner J, Sanderbrand S, Altincicek B, Weidemeyer C, et al. (1999) Inhibitors of the nonmevalonate pathway of isoprenoid biosynthesis as antimalarial drugs. Science 285: 1573–1576.
8. Nagamune K, Hicks LM, Fux B, Brossier F, Chini EN, et al. (2008) Abscisic acid controls calcium-dependent egress and development in *Toxoplasma gondii*. Nature 451: 207–210.
9. Kato M, Sasahara K, Ochi K, Akita H, Oishi T (1991) Asymmetric reduction of 2-aminobenzophenone using yeast, *Rhodosporidium toruloides*. Chem Pharm Bull 39: 2498–2501.
10. Trager W, Jensen JB (1976) Human malaria parasites in continuous culture. Science 193: 673–675.
11. Dobrowolski JM, Sibley LD (1996) Toxoplasma invasion of mammalian cells is powered by the actin cytoskeleton of the parasite. Cell 84: 933–939.
12. McFadden DC, Seeber F, Boothroyd JC (1997) Use of *Toxoplasma gondii* expressing beta-galactosidase for colorimetric assessment of drug activity *in vitro*. Antimicrob Agents Chemother 41: 1849–1853.
13. Yuan LC, Gulyas BJ (1981) An improved method for processing single cells for electron microscopy utilizing agarose. Anat Rec 201: 273–281.
14. Nair SC, Brooks CF, Goodman CD, Strurm A, McFadden GI, et al. (2011) Apicoplast isoprenoid precursor synthesis and the molecular basis of fosmidomycin resistance in *Toxoplasma gondii*. J Exp Med 208: 1547–1559.
15. Rademacher W (2000) Growth retardants: effects on gibberellin biosynthesis and other metabolic pathways. Annu Rev Plant Physiol Plant Mol Biol 51: 501–531.
16. Furuta R, Doi T (1994) Chiral separation of diniconazole, uniconazole and structurally related compounds by cyclodexrin-modified micellar electrokinetic chromatography. Electrophoresis 15: 1322–1325.
17. Hedden P, Phinney BO, MacMillan J, Sponsel VM (1977) Metabolism of kaurenoids by *Gibberella fujikuroi* in the presence of the plant growth retardant, N, N, N-trimethyl-1-methyl-(2′,6′,6′-trimethylcyclohex-2′-en-1′-yl) prop-2-enylammonium iodide. Phytochemistry 16: 1913–1917.
18. Palacpac NM, Hiramine H, Seto S, Hiramatsu R, Horii T, et al. (2004) Evidence that *Plasmodium falciparum* diacylglycerol acyltransferase is essential for intraerythrocytic proliferation. Biochem Biophys Res Commun 321: 1062–1068.
19. van Dooren GG, Marti M, Tonkin CJ, Stimmler LM, Cowman AF, et al. (2005) Development of the endoplasmic reticulum, mitochondrion and apicoplast during the asexual life cycle of *Plasmodium falciparum*. Mol Microbiol 57: 405–419.
20. Tanabe K (1983) Staining of *Plasmodium yoelii*-infected mouse erythrocytes with the fluorescent dye rhodamine 123. J Protozool 30: 707–710.
21. Divo AA, Geary TG, Jensen JB, Ginsburg H (1985) The mitochondrion of *Plasmodium falciparum* visualized by rhodamine 123 fluorescence. J Protozool 32: 442–446.
22. Mamoun BC, Prigge ST, Vial H (2010) Targeting the lipid metabolic pathways for the treatment of malaria. Drug Dev Res 71: 44–55.
23. Hartman M-A (1998) Plant sterols and the membrane environment. Trends Plant Sci 3: 170–175.
24. Hedden P, Kamiya Y (1997) Gibberellin biosynthesis: enzymes, genes and their regulation. Annu Rev Plant Physiol Plant Mol Biol 48: 431–460.
25. Yoshida Y (1988) Cytochrome P450 of fungi: primary target for azole antifungal agents. Curr Top Med Mycol 2: 388–418.
26. Miki T, Kamiya Y, Fukuzawa M, Ichikawa T, Sakurai A (1990) Sites of inhibition by a plant-growth regulator, 4′-chloro-2′-(alpha-hydroxybenzyl)-isonicotinanilide (inabenfide), and its related compounds in the biosynthesis of gibberellins. Plant Cell Physiol 31: 201–206.
27. Haines TH (2001) Do sterols reduce proton and sodium leaks through lipid bilayers? Prog Lipid Res 40: 299–324.
28. Guo DM, Venkatramesh M, Nes WD (1995) Developmental regulation of sterol biosynthesis in *Zea mays*. Lipids 30: 203–219.
29. Kaneda T (1991) Iso- and anteiso-fatty acids in bacteria: biosynthesis, function, and taxonomic significance. Microbiol Rev 55: 288–302.

30. Saar J, Kader J-C, Poralla K, Ourisson G (1991) Purification and some properties of the squalene-tetrahymanol cyclase from *Tetrahymena thermophila*. Biochim Biophysic Acta 1075: 93–101.
31. Welander PV, Hunter RC, Zhang L, Sessions AL, Summons RE, et al. (2009) Hopanoids play a role in membrane integrity and pH homeostasis in *Rhodopseudomonas palustris* TIE-1. J Bacteriol 191: 6145–6156.
32. Seo S, Tonda K, Uomori A, Takeda K, Hirata M (1993) Effect of sterol biosynthesis inhibitors, SSF-109, on cholesterol synthesis in isolated rat hepatocytes. Steroids 58: 74–78.
33. Jackson KE, Knonis N, Ferguson DJP, Adisa A, Dogovski C, et al. (2004) Food vacuole-associated lipid bodies and heterogeneous lipid environments in the malaria parasite, *Plasmodium falciparum*. Mol Microbiol 54: 109–122.
34. Pauls KP, Chambers JA, Dunbrofe EB, Thompson JE (1982) Perturbation of phospholipid membranes by gibberellins. New Phytol 91: 1–17.

OPEN ACCESS Freely available online

PLoS one

Clues to Evolution of the SERA Multigene Family in 18 *Plasmodium* Species

Nobuko Arisue[1], Satoru Kawai[2], Makoto Hirai[3], Nirianne M. Q. Palacpac[1], Mozhi Jia[1¤], Akira Kaneko[4,5,6], Kazuyuki Tanabe[7], Toshihiro Horii[1]*

1 Department of Molecular Protozoology, Research Institute for Microbial Diseases, Osaka University, Suita, Osaka, Japan, **2** Laboratory of Tropical Medicine and Parasitology, Dokkyo University School of Medicine, Mibu, Shimotsuga, Tochigi, Japan, **3** Department of Parasitology, Graduate School of Medicine, Gunma University, Maebashi, Gunma, Japan, **4** Department of Parasitology, Osaka City University Graduate School of Medicine, Osaka, Japan, **5** Island Malaria Group, Department of Microbiology, Tumor and Cell Biology, Karolinska Institutet, Stockholm, Sweden, **6** Institute of Tropical Medicine, Nagasaki University, Nagasaki, Japan, **7** Laboratory of Malariology, Research Institute for Microbial Diseases, Osaka University, Suita, Osaka, Japan

Abstract

SERA gene sequences were newly determined from 11 primate *Plasmodium* species including two human parasites, *P. ovale* and *P. malariae*, and the evolutionary history of SERA genes was analyzed together with 7 known species. All have one each of Group I to III cysteine-type SERA genes and varying number of Group IV serine-type SERA genes in tandem cluster. Notably, Group IV SERA genes were ascertained in all mammalian parasite lineages; and in two primate parasite lineages gene events such as duplication, truncation, fragmentation and gene loss occurred at high frequency in a manner that mimics the birth-and-death evolution model. Transcription profile of individual SERA genes varied greatly among rodent and monkey parasites. Results support the lineage-specific evolution of the *Plasmodium* SERA gene family. These findings provide further impetus for studies that could clarify/provide proof-of-concept that duplications of SERA genes were associated with the parasites' expansion of host range and the evolutionary conundrums of multigene families in *Plasmodium*.

Citation: Arisue N, Kawai S, Hirai M, Palacpac NMQ, Jia M, et al. (2011) Clues to Evolution of the SERA Multigene Family in 18 *Plasmodium* Species. PLoS ONE 6(3): e17775. doi:10.1371/journal.pone.0017775

Editor: Gordon Langsley, Institut national de la santé et de la recherche médicale - Institut Cochin, France

Received December 9, 2010; **Accepted** February 9, 2011; **Published** March 15, 2011

Funding: This work was supported by the Ministry of Education, Culture, Sports, Science and Technology grant (21570238 to N. A.; 20390120 to K.T.; 18073013 to T.H.) [http://www.mext.go.jp/english/]. The funders had no role in study design, data collection and analyses, decision to publish, or preparation of the manuscript.

Competing Interests: The authors have declared that no competing interests exist.

* E-mail: horii@biken.osaka-u.ac.jp

¤ Current address: Teaching and Research Group of Medical Parasitology, Department of Pathogenic Biology, Peking University Health Science Center, Beijing, China

Introduction

Malaria, caused by the genus *Plasmodium*, is one of the most serious infectious diseases prevalent in the tropics. There were an estimated 243 million cases and 863,000 malaria deaths in 2008 (WHO, 2009). The emergence of drug-resistant parasites has made its control more difficult than before and, thus, a better understanding of the biology of malaria parasites is required to gain insights into new effective control measures including malaria vaccines and new antimalarial drugs. The genome of *Plasmodium* presents basic information for this understanding. One of the prominent features of *Plasmodium* genomes is the presence of various unique multigene families, such as *the Plasmodium* interspersed repeats, *pir* [1]. The *pir* families are highly species-specific, suggesting evolution of lineage-specific immune evasion mechanisms. By far the best documented of multigene families is the *var* gene family of *P. falciparum*, the most virulent human malaria parasite. Products of *var* genes appear on the surface of infected erythrocytes and are involved in antigenic variation to evade host immunity. Other species-specific gene families encode proteins involved in host cell invasion, *e.g.* rhoptry proteins and parasite surface antigens, merozoite surface protein-3 and -7. In sharp contrast to a very large number (several hundreds) of rRNA gene family in other eukaryotes [2,3], *Plasmodium* has a very limited array (n = 4–7 units). Thus, *Plasmodium* possesses unique multigene family members in its genome with distinctive evolutionary conundrums.

Plasmodium also has the serine repeat antigen (SERA) multigene family that encodes proteins with a putative papain-like cysteine protease motif. In *P. falciparum*, SERA5 (Pfa-SERA5), one of nine SERAs, is a vaccine candidate now on phase Ib clinical trial in Uganda [4]. Serum antibodies against the N-terminal domain of Pfa-SERA5 in individuals living in malaria endemic areas protect infants from clinical malaria and inhibit *in vitro* parasite growth [4–7]. These studies and previous vaccine trials using laboratory animals [4,8–10] suggest the N-terminal domain of Pfa-SERA5 as a promising malaria vaccine candidate. Pfa-SERA5 (120 kDa) is abundantly produced at the late trophozoite to schizont stages of parasite development [7,11–12], is secreted together with other SERAs into the parasitophorous vacuole in an infected erythrocyte [7], and is processed into three fragments: the N-terminal domain (47 kDa), the central domain containing putative papain-like cysteine protease motif (56 kDa) and the C-terminal domain (18 kDa). The N-terminal 47 kDa fragment is further processed into two 25 kDa fragments, linked with the C-terminal 18 kDa fragment via disulfide bonding, and attach to the merozoite